TES-1/Tes and ZYX-1/Zyxin protect junctional actin networks under tension during epidermal morphogenesis in the *C. elegans* embryo

Allison M. Lynch*[1], Yuyun Zhu[1]*, Bethany G. Lucas[5], Jonathan D. Winkelman[6], Keliya Bai[7,10], Sterling C.T. Martin[2], Samuel D. Block[4,11] Mark M. Slabodnick[8,9], Anjon Audhya[4], Bob Goldstein[9], Jonathan Pettitt[7], Margaret L. Gardel[6], and Jeff Hardin[1,2,3,†]

[1]Program in Genetics, [2]Biophysics Program, [3]Department of Integrative Biology, and [4]Department of Biomolecular Chemistry, University of Wisconsin, Madison, WI 53706 USA
[5]Department of Biology, Regis University, 3333 Regis Boulevard, Denver, Colorado 80221 USA
[6]Institute for Biophysical Dynamics, University of Chicago, Chicago, IL 60637 USA
[7]University of Aberdeen, Institute of Medical Sciences Aberdeen AB25 2ZD UK
[8]Department of Biology, Knox University, Galesburg, Illinois, USA
[9]Department of Biology, University of North Carolina at Chapel Hill, Chapel Hill, North Carolina, USA

[10]Current address: Max-Planck Institute of Molecular Cell Biology and Genetics, Pfotenhauerstrasse 108, 01307, Dresden, Germany
[11]Current address: Koch Institute for Integrative Cancer Research, Massachusetts Institute of Technology, 77 Massachusetts Ave. Building 76-511, Cambridge, MA 02139 USA

*Co-first authors

†Author for correspondence:
Department of Integrative Biology, University of Wisconsin
1117 W. Johnson St. Madison, WI 53706 USA
email: jdhardin@wisc.edu

Abbreviations used in this study:
AJ, adherens junction
CCC, cadherin-catenin complex
CFB, circumferential filament bundle
DIC, differential interference contrast
LIM, Lin-11, Isl-1, Mec-3
PET, Prickle, Espinas, Testin
CR = cysteine-rich
SFSS = stress fiber strain site

Abstract

During embryonic morphogenesis, the integrity of epithelial tissues depends on the ability of cells in tissue sheets to undergo rapid changes in cell shape while preventing self-injury to junctional actin networks. LIM domain-containing repeat (LCR) proteins are recruited to sites of strained actin filaments associated with stress fibers in cultured cells [1-3], and are therefore promising candidates for mediating self-healing of actin networks at cell-cell junctions, but their roles in living organisms have not been extensively studied. Here, we establish roles for the *Caenorhabditis elegans* LCR proteins TES-1/Tes and ZYX-1/Zyxin at apical junctions during epithelial morphogenesis. TES-1 and ZYX-1 are recruited to apical junctions during embryonic elongation, when junctions are under tension; in genetic backgrounds in which embryonic elongation fails, junctional recruitment of both proteins is severely compromised. The two proteins display complementary patterns of expression: TES-1 is expressed mainly in lateral (seam) epidermal cells, whereas ZYX-1 is expressed in dorsal and ventral epidermal cells. *tes-1* and *zyx-1* mutant embryos display junctional F-actin defects, and loss of TES-1 strongly enhances tension-dependent injury of junctional actin networks in hypomorphic mutant backgrounds for cadherin/catenin complex components. Consistent with a role in stabilizing junctional actin networks during rapid cell shape change, the LCR regions of TES-1 and ZYX-1 are both recruited to stress fiber strain sites (SFSSs) in cultured vertebrate cells. Together, these data establish TES-1 and ZYX-1 as components of a multicellular, tension-sensitive system that stabilizes the junctional actin cytoskeleton during embryonic morphogenesis.

Introduction

Embryonic tissues require epithelial cell-cell adhesions that are both dynamic and strong. On the one hand, they must be dynamic, as cells rearrange and change shape to allow for the complex processes of morphogenesis, but on the other, cell-cell adhesions must be able to withstand contractile forces that threaten tissue integrity [4-7]. Thus, identifying factors that modulate junctional integrity is important for understanding embryonic morphogenesis. Here, we describe a novel modulatory role for the *C. elegans* Testin/Tes ortholog, TES-1, and the zyxin ortholog, ZYX-1, at cell-cell junctions.

Vertebrate Tes/testin (hereafter Tes) has an N-terminal CR domain, a PET (Prickle, Espinas and Testin) domain, and three C-terminal LIM (Lin11, Isl-1 & Mec-3) domains. Biochemical and structure-function analyses have suggested that the N terminus of Tes allows association with the actin cytoskeleton [8,9]. The LIM domains appear to allow association with heterologous binding partners[10,11], may be involved in mediating intracellular inhibition of Tes[12] and the PET domain may allow homodimerization of Tes via interaction with the LIM1-2 region [13].

Tes has been implicated in several actin-dependent processes. In cultured cells, Tes localizes to focal adhesions, integrin-based attachment sites linking intracellular actin stress fibers to sites of attachment to the extracellular matrix (ECM) [1,8,9,14]. Tes also appears to associate with cell-cell adhesions. Tes localizes to spot-like cell-cell contacts [10,15], where it colocalizes with cadherin/catenin complex (CCC) components [10]. Vertebrate zyxin can interact with Tes in vitro [9,11] and also localizes to adherens junctions [8,9,15-22]. Zyxin and other LIM domain proteins preferentially localize to natural rupture sites in bundled F-actin networks in cultured cells subjected to tension, where they are thought to allow rapid healing of ruptured

bundles [23-25]; reviewed in [1]. In cultured cells the LIM domains of zyxin, Tes, and other LIM domain proteins are sufficient for this response [2].

While previous work has examined the roles of Tes and zyxin in establishing and maintaining actin networks under stress in cultured cells, particularly at sites of cell-ECM attachment, surprisingly little work has been directed at the roles of these proteins at sites of epithelial cell-cell adhesion in an intact, developing organism. Despite careful analysis, a zyxin knockout mouse has no discernable epithelial phenotypes[26]. In *Drosophila* the zyxin homologue localizes to the subapical membrane in epithelia, where it has been implicated in a branch of the Hippo signaling pathway involving the non-classical cadherin, Fat and the apical myosin, Dachs[27]. Similarly, mouse testin interacts genetically and physically with the planar cell polarity (PCP) component Vangl2 in PCP-mediated organization of hair cells in the cochlea and vestibular system[15]. In neither of these cases, however, was zyxin or Tes functionally implicated in CCC-mediated adhesion events.

C. elegans epidermal morphogenesis provides a convenient system for studying the roles of proteins that modulate cadherin-dependent, epithelial cell-cell adhesion. Epidermal morphogenetic movements that require the CCC include (1) ventral enclosure, during which the embryo is encased in an epidermal monolayer [28] and new epidermal cell-cell junctions are formed [29]; and (2) the early phase of elongation, which involves a coordinated actomyosin-mediated contraction of the embryo, primarily driven by lateral (seam) epidermal cells [30,31]; reviewed in [32,33]. These contractile forces exert substantial tension on cell-cell junctions; the forces of contraction are transmitted via circumferential filament bundles (CFBs), large bundles of F-actin anchored at epidermal cell-cell junctions [30,34]. Anchorage of CFBs depends on the core components of the CCC: HMR-1/cadherin, HMP-2/β-catenin, and HMP-1/α-catenin [29]. Reduced

function of core CCC components coupled with removal of other adherens junctional proteins leads to catastrophic morphogenetic failure, predominantly during embryonic elongation [35-38]. Here, we describe the roles of TES-1/Tes and ZYX-1/zyxin in stabilizing the epidermal junctional proximal actin network that maintains the connection between the CCC and CFBs during periods of mechanical stress in the developing *C. elegans* epidermis.

Results and Discussion

We previously conducted a genome-wide RNAi screen in a sensitized HMP-1/α-catenin background, *hmp-1(fe4)*, and uncovered modulators of cell adhesion in *C. elegans* during morphogenesis [37]. In our initial screen, we identified a gene on chromosome IV, which when knocked down, potently enhanced the penetrance and severity of the *hmp-1(fe4)* phenotype [37] (Supplemental Video 1). Previously named TAG-224 (Temporarily Assigned Gene 224), we renamed the protein TES-1 because of its significant homology to the vertebrate protein Tes after examination of the predicted protein sequence using BLAST and ClustalW. ClustalW analysis indicates that TES-1 is approximately 35% identical and 64% similar to human Tes. Pfam analysis shows both proteins have a similar domain structure: an N-terminal PET domain followed by three C-terminal LIM domains (Fig. 1A).

TES-1 is an F-actin-binding protein that functionally interacts with hmp-1/α-catenin at the* C. elegans *apical junction

100% of *hmp-1(fe4); tes-1(RNAi)* embryos arrested during the elongation stage of morphogenesis with junctional actin defects that suggest a requirement for TES-1 during developmental stages requiring strong cell-cell adhesions (Fig. 1B-E). We also crossed a deletion allele, *tes-1(ok1036),* into *hmp-1(fe4)* worms and obtained a similar result: double homozygotes

exhibit 93.8% lethality and elongation arrest (n = 516 embryos examined). Moreover, *tes-1* RNAi enhanced lethality in a *hmp-2/β-catenin* hypomorph (*hmp-2(qm39)*; Fig. S1). Phalloidin staining demonstrated that *tes-1* RNAi exacerbated junctional proximal actin defects in a *hmp-1(fe4)* background (Fig. 1F-H). In 26 % of *hmp-1(fe4); tes-1(RNAi)* embryos (6 of 23 embryos examined via 4d microscopy) individual cells leaked out of the ventral midline, compared with 0% of *hmp-1(fe4)* homozygotes (0 of 22 embryos examined; significantly different, Fisher's exact test, p = 0.02). Since ventral enclosure involves the formation of nascent CCC-dependent junctions at the ventral midline[29], this result suggests that TES-1 is also involved in this process (Fig. 1E, arrow).

We next confirmed that, like vertebrate Tes [8,9], TES-1 directly binds F-actin by performing actin cosedimentation assays using recombinant TES-1 protein and found that TES-1 cosediments with F-actin (Fig. 1I). The extent of cosedimentation of TES-1 with F-actin was statistically indistinguishable from another well characterized junctional actin-binding protein in *C. elegans*, HMP-1/α-catenin [39] (Fig. 1J).

TES-1 localizes to apical junctions in the embryonic epidermis

To assess the expression pattern and subcellular localization of TES-1, we constructed an endogenously tagged version of *tes-1* fused to mNeonGreen (Fig. 2A). *mNG::tes-1* embryos, larvae, and adults were phenotypically indistinguishable from wildtype. In larvae, TES-1 was visible at alae, epidermal structures produced by larval seam cells; in adults, TES-1 is expressed in vulval tissues (data not shown). In early embryos, mNG::TES-1 was visible in epidermal cells, where its location is exclusively cytoplasmic. At the 2-fold stage of elongation, mNG::TES-1 puncta began to accumulate at sites of cell-cell contact. These clusters expanded and became

more evenly distributed along cell borders as elongation continued. Strikingly, mNG::TES-1 was maintained at seam-dorsal and seam-ventral, but not seam-seam borders (Fig. 2B, arrow).

To address the role of junctional components in localizing TES-1 in living embryos, we performed knockdown experiments in *mNG::tes-1* embryos followed by confocal microscopy. The effects of loss of function of *hmr-1*/cadherin on mNG::TES-1 localization were severe. In *hmr-1(RNAi)* embryos TES-1::GFP failed to be recruited to junctions (Fig. 2C). In contrast, *ajm-1(RNAi)* in embryos expressing mNG::TES-1 did not prevent localization of TES-1 to junctions (Fig. 2D). However, TES-1 foci did not spread to form a continuous, intense band as in wildtype, which may reflect the failure of *ajm-1(RNAi)* embryos to elongate successfully.

To determine whether mNG::TES-1 colocalizes with adhesion complexes, we performed colocalization experiments using endogenously tagged junctional proteins. The apicobasal distribution of TES-1 indicated that it colocalizes with the cadherin/catenin complex as opposed to the DLG-1/AJM-1 complex. Embryos expressing HMP-1/α-catenin::mScarletI and mNG::TES-1 displayed substantial overlap of HMP-1 and TES-1 (Fig. 2E), whereas there was little to no overlap with DLG-1/Discs large::dsRed, a component of the DLG-1/AJM-1 complex, which is basal to the CCC (Fig. 2F). Quantitative colocalization confirmed this assessment: Pearson's R value (above threshold) for TES-1/DLG-1 colocalization is 0.25, and for TES-1/HMP-1 is 0.58 (n = 10 junctions for each genotype; significantly different, $p < 0.0001$, unpaired Student's t-test). Partial localization of Tes with the CCC has likewise previously been reported in cultured vertebrate cells [10]. Although one study reported that vertebrate α-catenin and Tes can be coimmunoprecipitated [40], we were unable to coimmunoprecipitate TES with *C. elegans* CCC components in a generalized proteomics approach [41] or in directed coIP experiments (Fig. S2), suggesting that the interaction of TES-1 with the *C. elegans* CCC is

indirect. Alternatively, force-dependent interactions between LCR proteins and cell-cell junctions may be transient and weak, as suggested by a recent BioID study of zyxin [42], and thus difficult to demonstrate using traditional biochemical approaches.

TES-1 regulates actin networks during elongation

We next assessed why loss of TES-1 might enhance the *hmp-1(fe4)* phenotype. Since TES-1 binds F-actin and colocalizes with the CCC, we reasoned that TES-1 could stabilize CCC-dependent junctional proximal actin networks during morphogenesis, and that loss of *tes-1* function in an otherwise wild-type background might display sublethal defects in junctional F-actin architecture. Consistent with this possibility, when we examined F-actin organization in *tes-1(ok1036)* homozygous embryos (i.e., *tes-1(ok1036)* single mutants without the *fe4* mutation in the background) via phalloidin staining, we found defects absent in wild-type embryos (Fig. 2G-I). As compared to wild-type embryos (Fig. 2G), the majority of *tes-1(ok1036)* embryos displayed significantly narrower zones of junctional proximal actin (Fig. 2H; quantified in Fig. 2J). Additionally, we also observed more severe phenotypes, including gaps between CFBs, CFB collapse, and complete loss of preserved junctional-proximal actin (Fig. 2I). We classified actin defects into several categories based on these common phenotypes for the purposes of quantification: Class 1 (normal CFBs and junctional-proximal actin); Class 2 (reduced junctional-proximal actin); Class 3 (both reduced junctional-proximal actin and CFB organizational defects); and Class 4 (junctional-proximal actin absent and CFB organization defects). *tes-1(ok1036)* embryos displayed significantly higher percentages of Class II-IV embryos (Fig. 2K). We conclude that TES-1 stabilizes junctional-proximal actin during morphogenesis.

TES-1 requires its PET and LIM domains

To identify which subdomains are required for junctional targeting and function of TES-1 we analyzed the expression pattern of endogenously tagged *tes-1* deletions. Unlike full-length mNG::TES-1 (Fig. 3A), mNG::TES-1ΔPET localized along all seam cell borders in the epidermis (Fig. 3B). Deletion of the all three LIM domains simultaneously resulted in mNG::TES-1 localization along structures that appear to be CFBs (Fig. 3C). Because full-length mNG::TES-1 localized to cell-cell junctions, this result suggests that the latent ability of TES-1 to bind to CFBs is not normally manifest when the N terminal regions of the protein are present. These results are consistent with work on vertebrate Tes, which can co-immunoprecipitate actin [9] and localize via its N terminus in a non-mechanosensitive manner [13,40,43]. Line scans indicated that when either the PET or LCR domains were deleted, TES-1 was still extensively recruited to seam-dorsal and seam-ventral junctions (Fig. 3D), but embryos showed ectopic TES-1 junctional localization at seam-seam junctions (Fig. 3E). Deletion of the PET domain led to an increase in junctional vs. cytoplasmic signal compared to wildtype, while removal of all three LIM domains resulted in the opposite effect (Fig. 3F). These results indicate that both the LCR and PET domains are required for normal levels of junctional recruitment, in addition to targeting to specific junctions. One possiblilty is that an interaction between the PET and LCR domains restricts the domain-specific binding affinities of the PET and LCR domains; such an interaction has been proposed for vertebrate Tes based on biochemical assays[9].

We also expressed various TES-1::GFP deletion constructs in transgenic embryos (see Fig. S3A for a schematic of the full-length transgene used, as well as the genomic positions of the PET and LIM domains) and analyzed their localization and their ability to rescue embryonic viability in offspring from *hmp-1(fe4)/+; tes-1(ok1036)* mothers. Full-length TES-1::GFP, TES-

1ΔPET::GFP, and TES-1ΔLIM1-3 recapitulated the expression of endogenous knock-ins (Fig. S3B,C,G). Deletion of LIM1 (Fig. S3D) or LIM2 (Fig. S3E) both perturbed junctional localization similarly: each localized sporadically to epidermal junctions, including some seam-seam junctions. However, there was also localization at what appeared to be actin-containing structures in epidermal cells. Deletion of LIM3 rendered the GFP largely cytoplasmic (Fig. S3F). Importantly, TES-1::GFP rescued lethality seen in *tes-1(ok1036)/+; hmp-1(fe4)* embryos. *tes-1(ok1036)/+; hmp-1(fe4)* worms were extremely difficult to maintain due to *fe4* maternal effect; progeny of such worms exhibited 80% lethality (n = 20 embryos scored) and the addition of extrachromosomal TES-1::GFP reduced this lethality to 38% (n = 92 embryos scored). Significantly, *tes-1(ok1036); hmp-1(fe4)* worms could develop to adulthood, but only if they expressed *tes-1::gfp*, indicating the TES-1::GFP is functional.

Due to maternal effects and gonadal defects, assessing synergistic lethality of *tes-1::gfp* deletion constructs in tes-1(ok1036); *hmp-1(fe4)* homozygous mothers proved challenging. Fertile *tes-1(ok1036); hmp-1(fe4)* worms harboring *tes-1ΔLIM1::GFP* could not be obtained, but occasional *tes-1(ok1036); hmp-1(fe4)/+; tes-1ΔLIM1::GFP* embryos were able to grow to adulthood, but these adults were sterile. We therefore tested for the ability of subdomains of TES-1 to rescue synergistic lethality in *tes-1(ok1036); hmp-1(fe4)/+* embryos (Fig. S3H). TES-1ΔPET significantly rescued some embryonic lethality in this genetic background, but progeny had numerous defects, including germline malformations, protruding vulvae, and sterility. TES-1ΔLIM1-3, TES-1ΔLIM2, and TES-1ΔLIM2 were unable to rescue the 39% lethality observed among progeny of *tes-1(ok1036); hmp-1(fe4)/+* mothers. Overall, these results indicate that the LIM domains of TES-1 are crucial for *tes-1* function during morphogenesis.

While the deletion analysis indicated that the LIM domains are crucial for junctional targeting of TES-1, the difference in localization pattern of the ΔLIM3 and ΔLIM1-3 is curious, since the entire LCR region, with appropriate spacing between individual LIM domains, has been suggested to be crucial for F-actin binding[3,44]. Recently, it has been suggested that the LIM1-2 domain of vertebrate TES can engage in both heterophilic binding to proteins such as zyxin and homophilic dimerization via interaction with the PET domain of Tes [40]. Homodimerization of αE-catenin drives it away from adherens junctions [45,46]. While it is not currently known if homodimeric Tes is sequestered away from cell adhesion sites in a similar way, if it is this might explain the cytoplasmic accumulation of TES-1ΔLIM3::GFP in *C. elegans*. Deletion of LIM3 might favor homodimerization over heterophilic interactions of TES-1 with other binding partners. Alternatively, deletion of LIM3 may cause misfolding of the resulting truncated protein.

TES-1 localizes to junctions in a tension-dependent manner

Tes is required for the maintenance of stress fibers in cultured vertebrate cells[47], accumulates at "focal adherens junctions" (spot-like foci of cell-cell adhesion), in human vascular endothelial cells [10], and accumulates at stress fibers downstream of Rho signaling [43]. These data suggest that Tes might play tension-dependent roles in organizing the actin network at adherens junctions in epithelia during embryonic morphogenesis. During elongation of the *C. elegans* embryo, a coordinated change in the shape of epidermal cells drives elongation of the embryo to approximately 4-fold its original length [30]. The CCC anchors CFBs at junctions – specifically seam-ventral and seam-dorsal junctions – during this time, when the contractile forces driving elongation result in elevated tension at these junctional boundaries [29,34,48-50].

Given the localization of TES-1, we sought to test whether it is recruited to junctions in a tension-sensitive manner during embryonic elongation.

Because *hmr-1*/cadherin, *hmp-1*/*α-catenin*, and *hmp-2/β-catenin* homozygous null mutant embryos fail to progress past the two-fold stage of elongation, we could not assess whether disruption of TES-1::GFP recruitment to junctions is due primarily to physical absence of CCC components or because of the pre-elongation death of the embryos. In order to adjudicate between these possibilities we examined *hmp-1(fe4)* embryos expressing TES-1::GFP. The *fe4* lesion causes weaker binding of F-actin by HMP-1 and leads to less stable junctions[51]. *hmp-1(fe4)* embryos displayed a variable phenotype; while some embryos failed to elongate appreciably, other embryos extended to the 2-fold stage of elongation. We found that TES-1::GFP did not localize to junctions in *hmp-1(fe4)* embryos that failed to elongate past 1.5-fold (10 of 10 embryos imaged via spinning disc confocal microscopy; Fig. 3G,J), even in embryos that survived and hatched. However, TES-1::GFP did localize to junctions in the rare *hmp-1(fe4)* embryos that elongated to at least 2-fold their original length (5 of 5 embryos examined; significantly different; Fisher's exact test, $p = 0.0003$; Fig. S4A). The correlation between the extent of elongation of *fe4* embryos and the normal TES-1::GFP localization pattern suggests that TES-1 is only recruited to junctions that resemble those in normal embryos at the 2-fold stage.

To examine whether junctional tension affects the ability of TES-1::GFP to localize, we introduced the full-length TES-1::GFP into *let-502(sb118)* worms (Fig. 3H; Fig. S4C-D). Loss of LET-502/Rho kinase reduces actomyosin contractility in the epidermis and prevents elongation of *C. elegans* embryos. *let-502(sb118)* is a temperature-sensitive allele; when *let-502(sb1180); tes-1::gfp* embryos were imaged at permissive temperatures, TES-1::GFP localized

to junctions in a wild-type manner (Fig. S4C; quantified in Fig. 3J, *let-502(sb118)* ≥ 1.5x). However, when these embryos were reared at the restrictive temperature (25°C), TES-1::GFP remained entirely cytoplasmic in embryos that failed to elongate (Fig. 3H; quantified in Fig.3J, *let-502 (sb118)* 1.25x). We also attempted the converse experiment: loss of MEL-11/myosin phosphatase function results in excessively elongated embryos due to greater than normal epidermal contractility [49,50]. However, adhesion complexes undergo changes in morphology that made this converse experiment difficult to interpret. In MEL-11-depleted embryos, the initially continuous distribution of junctional TES-1::GFP was progressively lost, as TES-1::GFP became fragmented and pulled away from junctions into puncta (Fig. 3I). One possibility consistent with this result is that the excessive tension that develops in a *mel-11* loss-of-function background leads to collapse of junctional proximal actin around CFB insertion sites, including associated TES-1.

ZYX-1/zyxin localizes to junctions in a tension-dependent manner complementary to TES-1

Studies in vertebrate tissue culture cells indicate similar, but not entirely overlapping, localization of Tes and zyxin at spot adherens junctions [10,22]. Moreover, targeted interaction studies [9] and proteomics screens [40] suggest that the two proteins may physically associate, either directly or as part of a complex. We therefore set out to examine the role of *zyx-1* during embryonic elongation. First, we used an endogenous *zyx-1a* knock-in tagged with mNeonGreen[52] to assess *zyx-1* expression. In *C. elegans*, ZYX-1 has been reported to localize at muscle attachment sites[53,54] and at sites of cell-cell contact in the gastrulating embryo[52]. However, its localization at adherens junctions in the fully formed epidermis has not been reported. Endogenously tagged mNG::ZYX-1A (hereafter ZYX-1) showed a localization pattern partially

similar to mNG::TES-1, with strong localization at seam-dorsal and seam-ventral junctions in the epidermis during mid-late elongation. Strikingly, however, ZYX-1 showed a cellular pattern of expression complementary to that of TES-1: whereas mNG::TES-1 showed strong expression in seam cells, ZYX-1 was expressed strongly within non-seam cells (Fig. 4A).

Like mNG::TES-1, epidermally expressed transgenic ZYX-1::GFP colocalized with the cadherin-catenin complex, and its localization was disrupted by HMP-1 depletion (Fig. S5B-D). Given that the LCR domain of zyxin, which contains LIM1-3, is thought to be required for interaction with F-actin[3,44], we created an endogenously tagged ΔLIM1-3 strain. mNG::ZYX-1ΔLIM1-3 was much more weakly recruited to junctions (Fig. 4B; for quantification, see Fig. S5E). We did not identify *zyx-1* in our original *hmp-1(fe4)* enhancer screen[37] perhaps because the genome coverage was incomplete in the library we were using[37]. We therefore crossed *zyx-1(gk190)* into the *hmp-1(fe4)* background and found that loss of *zyx-1* function enhanced lethality to 100%. This enhancement could be rescued with a ZYX-1::GFP expressed under the control of an epithelial-specific promotor, *lin-26*, suggesting that its role in modulating cell adhesion is restricted to epithelia (Fig. S5A). We also produced strains in which GFP-tagged, truncated forms of ZYX-1 were stably expressed only in epidermal cells. Not surprisingly, a construct lacking all three LIM domains was unable to rescue (Fig. S5A). Intriguingly, however, a construct lacking LIM1 and LIM3 could very weakly rescue when overexpressed in the epidermis, suggesting that there may be a more stringent requirement for the middle of the LCR during morphogenesis. *hmp-1(fe4); zyx-1(gk190)* embryos could not be rescued to near 100% viability by a stably expressed epidermal ZYX-1::GFP that lacks the N terminus (Fig. S5A), indicating a role for the N terminus that is yet to be discovered. Finally, we assessed whether, as is the case for TES-1, junctional recruitment of endogenously tagged ZYX-1 is not favored under

conditions of reduced tension. We found that, like mNG::TES-1, mNG::ZYX-1 was much more weakly recruited to seam/non-seam junctions in *let-502(RNAi)* embryos (Fig. 4C; for quantification, see Fig. S5E).

Finally, we performed phalloidin staining on *zyx-1(gk190)* homozygotes. The defects we observed were more subtle than those in *tes-1(ok1036)* homozygotes (see Fig. 2G-K). We did not detect any observable effects on CFBs, but we did observe small ruptures in the junctional proximal actin network at seam-dorsal and seam-ventral boundaries in the embryonic epidermis not observable in controls (Fig. S6).

Both TES-1 and ZYX-1 can be recruited to strained actin fibers

Mammalian LIM domain proteins are recruited to strained actin fibers via their LIM domain-containing region [2,3,24]. One assay for this recruitment relies on laser irradiation of stress fibers to produce stress fiber strain sites (SFSSs) in culture mammalian cells expressing the LCR of a LIM domain protein of interest[44]. Since removal of the LIM domains of TES-1 and ZYX-1 resulted in abnormal recruitment to junctional actin networks in the epidermis, we tested whether the LCRs of TES-1 and ZYX-1 behave similarly. When transfected into mouse embryonic fibroblasts, ZYX-1(LIM1-3)::mCherry was recruited to SFSSs with kinetics similar to the LCR of full-length, eGFP-tagged *M. musculus* zyxin (Fig. 4D; quantified in Fig. 4E,H; for a movie of the entire cell, see Supplemental Video 2). Compared with full-length *M. musculus* GFP-zyxin in the same assay, recruitment of the TES-1 LCR is less pronounced, but significant compared to the mCherry negative control (Fig. 4F; quantified in Fig. 4G,I; for a movie of the entire cells, see Supplemental Video 3). Thus, the LCRs of these two *C. elegans* proteins can be recruited to sites of strained F-actin.

ZYX-1/zyxin and TES-1/Tes act largely independently during elongation

We next assessed the interdependence of TES-1 and ZYX-1 in the epidermis during embryonic elongation. When we crossed the *mNG::tes-1* knock-in into *zyx-1(gk190)* or *zyx-1 null* (*cp419*) [52] worms, we saw no change in localization to specific boundaries at the 3-4-fold stage (Fig. S7A-C), nor did we see mislocalization of mNG::ZYX-1 in *tes-1(ok1036)* mutants (Fig. S7D-E). We examined the localization of TES-1 and ZYX-1 in detail using coexpressed endogenously tagged proteins. TES-1 and ZYX-1 appeared to abut one another across cell-cell junctions (Fig. 4J, and they do not colocalize quantitively at junctions (Pearson's R above threshold = 0.0, 13 junctions measured). We next examined *tes-1; zyx-1* double loss-of-function embryos, using the *zyx-1* null allele (*cp419*). We did not see any obvious enhancement of lethality, but occasional *tes-1(syb5622); zyx-1(cp419)* animals showed minor body morphology defects that became less severe during larval molts (3 out of 30 embryos). Finally, based on previous studies of vertebrate homologues [9,11], we assessed the physical interaction of TES-1 and ZYX-1. While vertebrate Tes can physically interact with zyxin [9,11] and we were able to coIP TES-1 and ZYX-1 (Fig. S8A), we were only able to detect a very weak, substoichiometric interaction between TES-1 and ZYX-1 via coIP and pulldown of bacterially expressed proteins (Fig. S8B).

We conclude that TES-1 and ZYX-1 act largely independently during embryonic elongation, and that they act in support of the cadherin-catenin complex during this process. Our results are consistent with experiments in vertebrates, which show that while depletion of zyxin can reduce the amount of Tes at focal adhesions[9], Tes can still localize independently of zyxin[11]. Our results further suggest that loss of one of these LCR proteins in an otherwise wild-type

background is insufficient to decrease tension below the threshold required for recruitment of the other in the complementary group of epidermal cells.

In summary, our results suggest that two LCR proteins – ZYX-1 in non-seam cells and TES-1 in seam cells – perform broadly similar functions in bolstering cadherin-dependent connections to the junctional-proximal F-actin network during morphogenesis. A similar division of labor between these two cell types has been elegantly demonstrated previously in the case of non-muscle myosin and other proteins in a series of investigations[31,34,55,56]. A previous study in tissue culture cells suggested that a crucial phenylalanine (F66) is found in the LIM domains of proteins that show mechanosensitive recruitment to SFSSs [3]. There may be assay dependence regarding this requirement, however, as some of us showed previously that F66 is not required for recruitment of isolated LCT domains to SFSSs [44]. Notably, zyxin has the F66 feature, but Tes does not [3,44].

Our results indicate that *C. elegans* Tes LCR shows less avid recruitment to SFSS than the ZYX-1 LCR when expressed heterologously. Tes has recently been shown to be activated by Rho signaling, however [43]; since Rho activity is thought to be upregulated specifically in seam cells during embryonic elongation in *C. elegans* [55,57], there may be less functional difference in binding of TES-1 and ZYX-1 to strained actin in vivo. Whether ZYX-1 and TES-1 play subtly different roles at the subcellular level is an interesting avenue for future investigation.

Our results are consistent with a model in which actomyosin-mediated tension generated in elongating embryos leads to strain-dependent recruitment of TES-1 and ZYX-1 to junctions during elongation, stabilizing them against the rigors of mechanical stress during morphogenesis. In this sense, elongating epidermal cells in the *C. elegans* embryo are likely to be subject to "self-injury", as they must remodel their junctional-proximal actin networks during the dramatic

change in shape these cells undergo. It is likely that LIM-domain dependent stabilization of junctional proximal actin filaments is only one component of an apparatus that stabilizes and repairs such filaments. For example, our previous experiments indicated that UNC-94/tropomodulin is recruited to the same junctions, where it presumably protects minus ends of F-actin filaments from subunit loss[35]. Recruitment of TES-1 and ZYX-1 to these same junctions could stabilize CCC-dependent actin networks by allowing strained F-actin at the CCC to self-heal, by recruiting additional F-actin to these networks, or both.

Figures

Figure 1. TES-1 loss enhances phenotypes in hypomorphic CCC backgrounds. (A) Protein domain maps of *C. elegans* TES-1 and human Tes. TES-1 and Tes both contain N-terminal Prickle, Espinas, Testin (PET) domains and three C-terminal Lin-11, Isl-1, Mec-3 (LIM) domains. The *tes-1*(*ok1036)* allele removes LIM1-2 along with some intronic sequence and introduces a frameshift into the remainder of the coding region. (B-E) *tes-1(RNAi)* enhances the severity of morphogenetic defects in *hmp-1(fe4)* embryos. (B) Wild-type embryo imaged using Nomarski microscopy. (C) *tes-1(RNAi)* embryo. (D) *hmp-1(fe4)* embryo; bulges become apparent during embryonic elongation (t = 2 hr). (E) In *hmp-1(fe4); tes-1(RNAi)* embryos, cells leak out of the ventral midline (t = 1 hr), and all embryos die with severe elongation defects (t = 2 hr). Scale bar = 10 μm. (F-H) *tes-1(RNAi)* enhances the severity of actin defects in *hmp-1(fe4)* embryos. Phalloidin staining of wild-type (F), *hmp-1(fe4)* (G), and *hmp-1(fe4); tes-1(RNAi)* (H) embryos. Bright signal is muscle (yellow arrowheads). Wild-type embryos maintain a population of junctional proximal actin along cell borders and dorsal and ventral epidermal cells in elongated embryos contain circumferential actin filament bundles (CFBs) that are evenly spaced. *hmp-1(fe4)* embryos also typically maintain junctional proximal actin; however, their CFBs are less evenly spaced, and sometimes clump together (white arrowhead). *hmp-1(fe4); tes-1(RNAi)* embryos display clumping of CFBs (white arrowhead) and a complete lack of junctional proximal actin. CFBs appear to have been torn away from the junction, leaving bare zones devoid of F-actin (white arrow). Scale bar = 10 μm. (I) TES-1 binds to F-actin in an actin co-sedimentation assay. Full-length TES-1 remains in the supernatant fraction (S) when incubated without F-actin. However, TES-1 is detected in the pellet fraction (P) when incubated with 5 μM F-actin. (J) Quantification of TES-1 found in the pellet after incubation with F-actin. Bovine

Serum Albumin (BSA) served as a negative control and SUMO::HMP-1 as a positive control. TES-1 bound to F-actin significantly more than BSA did (two replicates; ** = $p < 0.01$, unpaired Student's T test).

Figure 2. TES-1 localizes to sites of cell-cell attachment during embryonic elongation. (A) A schematic of the endogenous mNG::TES-1 knock-in strain used in this study. (B) mNG::TES-1 localizes strongly to seam-dorsal and seam-ventral boundaries (arrow). (C) *hmr-1(RNAi)* completely prevents mNG::TES-1 localization at junctions. (D) *ajm-(RNAi)* does not influence the ability of mNG::TES-1 to localize to junctions (arrow). Scale bar = 10 μm. (E) mNG::TES-1 co-localizes with endogenous HMP-1::mScarletI. (F) mNG::TES-1 does not co-localize with DLG-1::dsRed. Insets in (E) and (F) show magnifications of boxed regions. Scale bar = 10 μm. (G-I) Fixed and phalloidin stained embryos. Bright staining is muscle (arrowhead). Scale bar = 10 μm. (G) Wild-type embryos exhibit parallel circumferential filament bundles (CFBs, blue box inset) and retain junctional-proximal actin (green box inset). (H) Approximately half the *tes-1(ok1036)* embryos exhibit reduced junctional-proximal actin although CFB organization looks normal. (I) *tes-1(ok1036)* embryos also exhibit more severe phenotypes including gaps and clumping of CFBs (blue box) and a complete loss of junctional-proximal actin (green box). (J) Width of junctional proximal actin at seam-non-seam boundaries measured from phalloidin stained specimens (wildtype: n = 14 junctions; *tes-1(ok1036)*: n = 16 junctions; **** $p < 0.0001$, unpaired Student's T-test). (K) Quantification of phalloidin staining phenotypes. Class 1 embryos have normal CFBs and junctional-proximal actin. Class 2 embryos have reduced junctional-proximal actin. Class 3 embryos have reduced junctional-proximal actin and CFB organization defects and Class 4 embryos have no retained junctional-proximal actin

and CFB organization defects (wildtype: n = 16 embryos; *tes-1(ok1036)*: n = 40 embryos; **** = $p < 0.0001$, Freeman-Halton extension to Fisher's exact test).

Figure 3. TES-1 localization requires its PET and LCR domains. For relevant domains of TES-1, see Figure 1A. (A) Full-length endogenous mNG::TES-1 localizes to dorsal-seam and ventral-seam cell boundaries in the epidermis prominently by the two-fold stage. (B) Unlike full-length mNG::TES-1, mNG::TES-1ΔPET localizes along all seam cell borders in the epidermis, including seam-seam borders (arrows). There is also localization at what appear to be actin-containing structures in epidermal cells. (C) Deletion of LIM1-3 perturbs junctional localization: mNG::TES-1ΔLIM1-3 localizes sporadically to epidermal junctions, including seam-seam junctions (arrow). However, there is also localization to actin networks in seam cells and along structures that appear to be CFBs in non-seam cells. Scale bar = 10 μm. (D-E) Line scans of mNG::TES-1 signal across dorsal-seam and ventral-seam cell boundaries (D; position of scans indicated by white lines in A-C) and seam-seam boundaries (E; yellow lines in A-C) for full-length (WT) *mNG::tes-1*, *mNG::tes-1ΔPET*, and *mNG:: ΔLIM1-3* embryos. (F) Junctional/cytoplasmic signal for mNG::TES-1 (n = 12 junctions), mNG::TES-1ΔPET (n = 10), and mNG::TES-1ΔLIM1-3 (n = 10). ** = $p < 0.01$, **** = $p < 0.0001$, unpaired Student's T-test. (G-I) TES-1::GFP localization in elongation-defective transgenic embryos expressing TES-1::GFP. (G) In *hmp-1(fe4)* embryos that do not elongate past 1.5-fold before failing, TES-1::GFP does not localize to junctions, and instead remains entirely cytoplasmic (arrow). Yellow arrowhead indicates the characteristic Humpback phenotype. See Fig. S4A for images of *fe4* embryos that partially elongate. (H) In *let-502(sb118ts); tes-1::gfp* embryos reared at the restrictive temperature ("shifted"), the LET-502 protein is inactivated, embryos fail to elongate,

and TES-1::GFP never accumulates along epidermal junctions. Unshifted embryos display normal development and TES-1::GFP localizes to junctions as in wildtype (Fig. S4C). (I) In *mel-11(RNAi); tes-1::gfp* embryos, TES-1::GFP is pulled away from junctions in long extensions from epidermal cell borders. In embryos that elongate normally TES-1::GFP junctional localization is not affected (not shown). Scale bars = 10 μm. (J) Junctional/cytoplasmic ratio of TES-1::GFP in wild-type embryos at ≥ 2.5-fold stage of elongation (n = 17 junctions), *hmp-1(fe4)* embryos at 1.25-fold stage of elongation (n = 32) and *let-502(RNAi)* embryos at 1.25x (n = 23) and ≥ 1.5x (n = 33) stages of elongation. ** = $p < 0.01$, *** = $p < 0.001$, **** = $p < 0.0001$, unpaired Student's T-test.

Figure 4. ZYX-1 is also recruited to junctions during elongation and both ZYX-1 and TES-1 are recruited to strained actin filaments. (A) mNG::ZYX-1 is recruited to both dorsal-seam and seam-ventral junctions (white arrow), and it also colocalizes with CFBs after the two-fold stage (yellow arrowhead). (B) In *mNG::zyx-1ΔLIM1-3* embryos ZYX-1 is largely absent from junctions and is not recruited to CFBs. (C) *let-502 (RNAi)* embryos partially lose junctional localization of mNG::ZYX-1. Scale bars = 10 μm. (D-I) Recruitment of TES-1 LCR::mCherry and ZYX-1 LCR::mCherry to stress fiber strain sites (SFSS) in transfected mouse embryonic fibroblasts. (D) Representative kymographs of laser-induced recruitment of the ZYX-1 LCR::mCherry and mouse GFP::Zyxin to SFSS. For a timelapse sequence of the entire cell, see Supplemental Movie 2. White dashed and gray solid lines indicate where fluorescence and distance were measured. Dashed gray vertical line indicates t_0, when strain is first observed. (E) Quantification of GFP and mCherry accumulation over time in the kymograph from (D). (F) Representative kymographs of laser-induced recruitment of TES-1 LCR::mCherry and mouse GFP::Zyxin to SFSS. For a timelapse sequence of the entire cell, see Supplemental Movie 3. (G)

Quantification of GFP and mCherry accumulation over time in the kymograph from (F). (H-I) Intensity of *C. elegans* ZYX-1 LCR::mCherry (H) and *C. elegans* TES-1 LCR::mCherry (I) relative to full-length mouse GFP::Zyxin present in the same cells. Blue dots in each graph represent mCherry alone relative to GFP::MmZyx. TES-1 LCR::mCherry accumulates markedly ($p=0.023$, $n>10$) but to a lesser extent than MmZyx, error bars indicate 95% confidence intervals.

Supplemental Table 1. **Strains used in this study.**

Supplemental Table 2. Primer sequences for CRISPR experiments performed in this study.

Supplemental Figure 1. Depletion of TES-1 enhances defects in a *hmp-2* hypomorph. (Top) *hmp-2(qm39)* embryos are viable and display subtle body morphology defects. (Bottom) In *hmp-2(qm39); tes-1(RNAi)* embryos, cells leak out of the ventral midline in terminally arrested embryos (right panel, arrow). Scale bar = 5 μm.

Supplemental Figure 2. TES-1 cannot coimmunoprecipitate HMP-1/α-catenin. (A-B) TES-1::GFP was immunoprecipitated from an extract of mixed stage embryos, and the resulting proteins were blotted and probed with anti-GFP and anti-HMP-1 antibodies. (A) TES-1::GFP is substantially enriched in the IP fraction, demonstrating that anti-GFP antibodies can coIP TES-1::GFP. (B) Although in a parallel preparation HMP-1 can be detected in the total lysate, pellet and wash fractions, it is undetectable in the IP fraction**.**

Supplemental Figure 3. **Assessment of functional importance of specific TES-1 domains using transgenic rescue.** (A) A schematic of the full-length TES-1::GFP driven by its full-

length endogenous promoter used in this study. (B) Full-length TES-1::GFP localizes to dorsal-seam and ventral-seam cell boundaries in the epidermis (arrow). (C) Unlike full-length TES-1::GFP, TES-1ΔPET::GFP localizes along all seam cell borders in the epidermis, including seam-seam borders (arrows). Deletion of LIM1 (D) or LIM2 (E) both perturb junctional localization similarly: each localizes sporadically to epidermal junctions, including some seam-seam junctions. However, there is also localization at what appeared to be actin-containing structures in epidermal cells. (F) Deletion of LIM3 renders the GFP entirely cytoplasmic. (G) Deletion of all three LIM domains simultaneously results in GFP localization along structures that appear to be CFBs. (H) Rescue of embryonic lethality in progeny of *tes-1(ok1036); hmp-1(fe4)/+* hermaphrodites. * = significantly different from non-transgenic animals ($p < 0.05$, Fisher's exact test).

Supplemental Figure 4. TES-1::GFP is only recruited to cell boundaries in elongating cells. (A) In *hmp-1(fe4)* embryos that successfully elongate to two-fold, TES-1::GFP accumulates along seam cell junctions (white arrow). (B) In *hmp-1(fe4)* embryos that do not elongate past 1.5-fold before failing, TES-1::GFP does not localize to junctions, instead remaining entirely cytoplasmic. Same embryo as Fig. 3F. (C) In *let-502(sb118ts); tes-1::gfp* embryos reared at the permissive temperature ("unshifted"), development is normal and TES-1::GFP localizes to junctions as in wildtype. (D) In temperature-shifted embryos, the LET-502 protein is inactivated, embryos fail to elongate, and TES-1::GFP never accumulates along epidermal junctions. Same embryo as Fig. 3G. Scale bars = 10 μm.

Supplemental Figure 5. **ZYX-1 function is required in a *hmp-1(fe4)* background, ZYX-1 colocalizes with the cadherin/catenin complex, and ZYX-1 junctional localization requires HMP-1 function.** (A) Rescue of synthetic lethality in *hmp-1(fe4); zyx-1(gk190)* homozygotes by *zyx-1::gfp* transgenes (> 2000 progeny scores for each genotype). Full-length ZYX-1::GFP strongly rescues. (B) Colocalization of HMR-1::GFP and ZYX-1::mCherry in otherwise wild-type embryos along a junctional boundary in seam cells during elongation. (C) Lack of colocalization of ZYX-1::GFP and DLG-1::RFP in otherwise wild-type embryos along a junctional boundary in seam cells during elongation. (D) Expression of ZYX-1::GFP and DLG-1::RFP in a *hmp-1(zu278)* homozygous embryo with the characteristic Humpback phenotype. DLG-1 localized to junctions in a superficial optical plane (arrows), but ZYX-1 does not. Scale bars = 5 μm. (E) Junctional/cytoplasmic signal for mNG::ZYX-1 (n = 10 junctions), mNG::ZYX-1ΔLIM1-3 (n = 10), and mNG::ZYX-1; *let-502(RNAi)* embryos (n = 11). * = $p < 0.05$, **** = $p < 0.0001$, unpaired Student's T-test.

Supplemental Figure 6. Loss of *zyx-1* function leads to defects in junctional proximal actin. (A-B) Fixed and phalloidin stained embryos. Bright staining is muscle (arrowhead). Scale bar = 5 μm. (A) Wild-type embryos exhibit parallel circumferential filament bundles (CFBs, blue box inset) and retain junctional-proximal actin (green box inset). (B) Some *zyx-1(gk190)* embryos exhibit ruptures in the junctional-proximal actin network (white arrows) although CFB organization looks normal. (C) Quantification of junctional proximal actin defects. Wildtype: n = 17 junctions; *zyx-1(gk190)*: n = 33; ** = $p < 0.01$, Fisher's exact test.

Supplemental Figure 7. TES-1 and ZYX-1 junctional localization occur independently. (A-C). Junctional localization of mNG::TES-1 in (A) otherwise wild-type, (B) *zyx-1(gk190)*, and (C)

zyx-1(cp419[Pmyo-2>GFP]), a CRISPR-induced null allele. There is no obvious disruption of TES-1 recruitment. (D-E) Junctional localization of mNG::ZYX-1A in (D) otherwise wild-type and (E) *tes-1(ok1036)* embryos. There is no obvious disruption of ZYX-1 recruitment. Scale bars = 10 μm.

Supplemental Figure 8. TES-1 binds weakly to ZYX-1/zyxin. (A) Co-immunoprecipitation of TES-1 and ZYX-1. TES-1-GFP was immunoprecipitated from an extract of mixed stage embryos, and the resulting protein was blotted and probed with anti-GFP and anti-ZYX-1 antibodies. ZYX-1 is substantially enriched in the IP fraction. (B) Pulldown using recombinant ZYX-1/zyxin and TES-1/Tes. Extracts of bacteria expressing MBP-1-ZYX-1 were incubated with either GST or GST-TES-1. The resulting mixture was purified using glutathione beads, blotted, and probed using anti-MBP antibodies. MBP-ZYX-1 and TES-1-GST interact weakly at substoichiometric levels.

Supplemental Video 1. Time lapse movie comparing *hmp-1(fe4*) homozygous and *hmp-1(fe4); tes-1(RNAi)* embryos. The latter fail consistently during early elongation, and all develop the Humpback phenotype. Time is shown in hours:minutes.

Supplemental Video 2. Time lapse movie showing laser induction of a stress fiber strain site (SFSS) in a representative zyxin $^{-/-}$ mouse embryo fibroblast (MEF) rescued with stably integrated *M. musculus* GFP-zyxin and transiently transfected with a construct encoding ZYX-1 LCR::mCherry corresponding to Fig. 4D. White box show where light was targeted, and white arrows denote developing SFSS. Time is shown in minutes:sec.

Supplemental Video 3. Time lapse movie showing laser induction of a stress fibert strain site (SFSS) in a representative zyxin $^{-/-}$ mouse embryo fibroblast (MEF) rescued with stably integrated *M. musculus* GFP-zyxin and transiently transfected with a construct encoding TES-1 LCR::mCherry corresponding to Fig. 4F. White box show where light was targeted, and white arrows denote developing SFSS. Time is shown in minutes:sec.

Materials and Methods

Nematode Strains and Genetics

C. elegans strains were maintained using standard methods [58]. Bristol N2 was used as wildtype. Additional strains used in this study are listed in Supplemental Table 1.

Plasmids

A ~5kb genomic sequence containing 2kb promoter and entire genomic region of *tes-1* was PCR amplified using Phusion polymerase (NEB). The primers used were: 5' GCGTCGACGAGTTTTTGTCAAGAGTAAGAC and 3' GCCCCGGGATCAACTGATCATCCGGATTCG. The PCR product was digested with *SalI* and *SmaI* and ligated into a similarly digested Fire lab vector pPD95.75, which contains the GFP sequence. A frameshift was repaired via PCR to generate a *Ptes-1(2kb)::tes-1::gfp* construct (pAML224). To generate *Ptes-1(5kb)::tes-1::gfp*, additional promoter sequence was PCR amplified using Phusion polymerase. The primers used were: 5' GCCTGCAGGAAGACAACGCTTGTCAAGAAT and 3' GCGTCGACATTTTGCCCTCGAAATGCAATAC. The PCR product and pAML224 were digested using *PstI* and *SalI* and ligated together to generate pAML224v2. The identity of pAML224v2 was confirmed via sequencing. Domain deletions were performed using circle PCR as described previously [37].

CRISPR

mNG::TES-1 worms were generated via plasmid-based CRISPR/Cas9 [59] using repair templates cloned using SapTrap cloning [60]. All domain deletions mutations (PHX strains) were generated

by SunyBiotech (Fujian, China). Guides, homology arms primers, and single-stranded repair templates for all CRISPR/Cas9 editing can be found in Supplementary Table 2.

Microinjection

DNA was microinjected into worms as described previously [61]. Briefly, injection mixes consisting of 5ng/µl of transgenic *tes-1* DNA constructs, 20 ng/µl of junk DNA (F35D3) and 75 ng/µl of *rol-6(su1006)* transgenic marker DNA were microinjected into both gonads of hermaphrodites. Progeny were screened for the presence of *rol-6(su1006)*, and stable lines were established by passaging of worms. Purified *zyx-1* deletion construct DNA (100ng/ml) was mixed with coinjection markers pRF4 (200ng/ml), Cbr-unc-119(+) (30ng/ml), and Pmyo-2::dTomato (5ng/ml) diluted in sterile water. At least two stable lines from each injected transgene were. used to analyze expression patterns.

Injection RNA interference was performed as described previously [62]. dsRNA was generated using an Ambion T7 and/or T3 Megascript kits; templates included C10H11.9 (*let-502*), C06C3.1 (*mel-11*), yk662b10 (*hmr-1*), yk285a2 (*ajm-1*), and yk1054c06 (*zyx-1*) (NEXTDB, http://nematode.lab.nig.ac.jp/).

Antibody and Phalloidin Staining

Immunostaining was performed using freeze-cracking [63]. Staining was performed as described previously [64]. Embryos were mounted onto poly-L-lysine-coated ring slides and incubated with primary antibodies in PBST and 5% non-fat dry milk overnight at 4°C. Embryos were then

incubated with secondary antibodies in PBST and 5% non-fat dry milk for approximately three hours at room temperature. The following primary antibodies were used: 1:1000 mouse-anti-GFP (Invitrogen), 1:1000 rabbit-anti-GFP, 1:4000 polyclonal rabbit-anti-HMP-1, 1:4000 polyclonal rabbit-anti-HMR-1 and 1:200 monoclonal mouse-anti-AJM-1 (MH27). The following secondary antibodies were used: 1:50 anti-rabbit IgG Texas Red, 1:50 anti-rabbit FITC, 1:50 anti-mouse Texas Red and 1:50 anti-mouse FITC.

Phalloidin staining of mutant and wild-type embryos was used to visualize actin in fixed embryos [29]. Embryos were mounted on poly-L-lysine-coated ring slides and fixed using the following: 4% paraformaldehyde, 0.1 mg/mL lysolecithin, 48 mM Pipes pH 6.8, 25 mM Hepes pH 6.8, 2 mM $MgCl_2$, and 10 mM EGTA for 20 minutes at room temperature. 1:20 Phalloidin-488 was incubated with embryos at room temperature for 90 minutes. Images of stained embryos were acquired as described below.

For co-immunostaining and phalloidin staining, embryos were gathered in a 1.5 mL Eppendorf tube and permeabilized with a solution of 4% paraformaldehyde, 10% Triton-X-100, 48 mM Pipes pH 6.8, 25 mM Hepes pH 6.8, 2 mM $MgCl_2$ and 10mM EGTA for 20 minutes at room temperature. Embryos were incubated overnight in PBST+5% dry milk+1:1000 rabbit-anti-GFP at 4C on a nutator. Secondary antibodies (1:10 Phalloidin-666 and 1:50 anti-rabbit FITC) were incubated for 2 hours at room temperature. Images of stained embryos were acquired as described below.

Confocal Microscopy

Spinning-disc confocal images of *tes-1* transgenics were acquired with a Z-slice spacing of 0.2μm for imaging of actin, 0.3 μm for embryos stained for both GFP and actin, and 0.5μm for

all other imaging using either Perkin Elmer Ultraview or Micromanager software [65,66] and a Nikon Eclipse E600 microscope connected to a Yokogawa CSU10 spinning disk scanhead and a Hamamatsu ORCA-ER charge-coupled device (CCD) camera. Junctional/cytoplasmic signal measurements were performed as described previously [67]. Fisher's exact test calculations were performed online at https://www.socscistatistics.com/tests/fisher/default2.aspx or using GraphPad Prism v. 9.0 software (GraphPad Software, San Diego, California USA, www.graphpad.com). The extension of Fisher's exact test to a 4 x 2 contingency table[68] was performed online at http://vassarstats.net/fisher2x4.html. Other statistical analyses were performed using GraphPad Prism. For *zyx-1* transgenics, imaging was carried out using a Zeiss LSM 710 laser scanning confocal microscope equipped with 10x and 63x oil lenses.

For endogenous knock-ins, imaging was performed using a Dragonfly 500 spinning disc confocal microscope (Andor Corp.), mounted on a Leica DMi8 microscope, equipped with a Zyla camera and controlled by Fusion software (Andor Corp.). Images were collected using 0.18 µm slices with a 100×/1.3 NA oil immersion Leica objective at 20°C.

Colocalization Analysis

Colocalization analysis was performed in Fiji using Just Another Colocalization Plugin (JACoP; https://imagej.nih.gov/ij/plugins/track/jacop.html) [69]. 5 focal planes from >10 junctional segments were combined into single stacks for each genotype. Maximum intensity Z projections were obtained, and automated Costes thresholding within JACoP was visually confirmed in each case. Significant difference in Pearson's R for colocalizations was assessed using the online Z calculator available at http://vassarstats.net/rdiff.html

DIC Imaging

Four dimensional DIC movies were gathered on either a Nikon Optiphot-2 connected to a QImaging camera or an Olympus BX5 connected to a Scion camera. Mounts were made as previously described (Raich et al., 1999). ImageJ plugins (http://worms.zoology.wisc.edu/research/4d/4d.html) were used to compress and view movies.

Protein Expression and Purification

GST- and SUMO-His-tagged proteins were expressed in BL21-Gold(DE3) *Escherichia coli* cells and purified as described [51,70]. Cells were induced with 0.1mM IPTG at 18°C for 16 hours. Wash and elution buffers were as follows: GST wash (1X PBS, 500mM NaCl, 0.1% Tween-20, and 1mM DTT), GST elution (50mM Tris pH 8.0, 0.3% glutathione, 150mM NaCl), His wash (50mM Na-Phosphate pH 8.0, 300mM NaCl, 0.1% Tween-20, 10mM Imidazole), and His elution (250mM Imidazole, 100mM NaCl, 10% glycerol, 50mM Hepes pH 7.6). For actin-pelleting assays, the GST tag was cleaved from GST-TES-1 using ProTEV Plus (Promega), according to manufacturer's instructions.

Actin-Pelleting Assays

Actin co-sedimentation assays were performed as described previously [51]. Briefly, 5μM purified, cleaved proteins (quantified via a Bradford Assay) were incubated at room temperature for one hour with 0 or 5μM polymerized chicken F-actin (Cytoskeleton, Inc.). BSA was used a negative control, and SUMO-His-HMP-1 [41] was used as a positive control. Samples were then centrifuged at 100,000 rpm for 20 min at 4°C in a TLA-120.1 rotor using a Beckman Optima

tabletop ultracentrifuge. Samples were run on 12% SDS-PAGE gels, stained with Coomassie Brilliant Blue, and bands were quantified using ImageJ.

Co-immunoprecipitations and Western Blots

C. elegans expressing TES-1::GFP were grown in liquid culture as previously described [71]. Co-immunoprecipitations were completed as in [35]. Western blots were performed as described previously [72], using rabbit anti-GFP, rabbit anti-HMP-1 [41] and mouse anti-ZYX-1 [73] primary antibodies and Li-COR IRDye® secondary antibodies to detect proteins.

Stress fiber strain site assay

A *tes-1 LCR::mCherry* construct was designed and expressed using the procedures described in detail by Winkelman *et al.* [2]. Briefly, a synthetic gBlock DNA encoding a mammalian codon-optimized version of the LIM1-3 domain of TES-1 was ordered from IDT (Coralville, Iowa) and cloned into a CMV-driven expression vector that fused the C-terminus of LCR(Tes) to mCherry, and used to transfect zyxin $^{-/-}$ mouse embryo fibroblast cells (MEFs) rescued with stably integrated GFP-zyxin. Transfected MEFs were imaged on an inverted Nikon Ti-E microscope (Nikon, Melville, NY) with a Yokogawa CSU-X confocal scanhead and Zyla 4.2 sCMOS Camera (Andor, Belfast, UK). A 405 nm laser coupled to a Mosaic digital micromirror device (Andor) was used to locally damage stress fibers. Kymography of TES-1(LIM1-3)::GFP was performed using ImageJ as described in [2].

Acknowledgements

Some strains were provided by the *C. elegans* Genetics Center, which is funded by the NIH Office of Research Infrastructure Programs (P40 OD010440). cDNA clones for *hmr-1, ajm-1, zyx-1, zoo-1, hmp-1, and tes-1* (yk collection) were provided by Yuji Kohara (National Institute of Genetics). AL, YZ, BL, SM, and JH were supported by NIH grant R01GM058038 awarded to JH. BM was supported by a Gilliam Fellowship from the Howard Hughes Medical Institute, and by an Advanced Opportunities Fellowship and a COVID-19 dissertation completion fellowship from the University of Wisconsin-Madison. SB and AA were supported by NIH grant R35GM134865 awarded to AA. JW was supported by NIH grant F32GM122372 and by NIH grant R01GM104032 and Army Research Office Multidisciplinary University Research Initiative W911NF1410403 awarded to MG. BG and MMS were supported by NIH MIRA R35GM134838 awarded to BG and NIH F32GM119348 awarded to MMS. Some strains were provided by the *Caenorhabditis* Genetics Center (CGC; https://cbs.umn.edu/cgc/home), which is funded by the NIH Office of Research Infrastructure Programs (P40 OD010440).

References

1. Smith, M.A., Hoffman, L.M., and Beckerle, M.C. (2014). LIM proteins in actin cytoskeleton mechanoresponse. Trends Cell Biol *24*, 575-583. 10.1016/j.tcb.2014.04.009.
2. Winkelman, J.D., Anderson, C.A., Suarez, C., Kovar, D.R., and Gardel, M.L. (2020). Evolutionarily diverse LIM domain-containing proteins bind stressed actin filaments through a conserved mechanism. Proc Natl Acad Sci U S A. 10.1073/pnas.2004656117.
3. Sun, X., Phua, D.Y.Z., Axiotakis, L., Jr., Smith, M.A., Blankman, E., Gong, R., Cail, R.C., Espinosa de Los Reyes, S., Beckerle, M.C., Waterman, C.M., and Alushin, G.M. (2020). Mechanosensing through Direct Binding of Tensed F-Actin by LIM Domains. Dev Cell *55*, 468-482 e467. 10.1016/j.devcel.2020.09.022.
4. Charras, G., and Yap, A.S. (2018). Tensile Forces and Mechanotransduction at Cell-Cell Junctions. Curr Biol *28*, R445-R457. 10.1016/j.cub.2018.02.003.
5. Mege, R.M., and Ishiyama, N. (2017). Integration of Cadherin Adhesion and Cytoskeleton at Adherens Junctions. Cold Spring Harb Perspect Biol *9*. 10.1101/cshperspect.a028738.
6. Pinheiro, D., and Bellaiche, Y. (2018). Mechanical Force-Driven Adherens Junction Remodeling and Epithelial Dynamics. Dev Cell *47*, 3-19. 10.1016/j.devcel.2018.09.014.
7. Wickstrom, S.A., and Niessen, C.M. (2018). Cell adhesion and mechanics as drivers of tissue organization and differentiation: local cues for large scale organization. Curr Opin Cell Biol *54*, 89-97. 10.1016/j.ceb.2018.05.003.
8. Coutts, A.S., MacKenzie, E., Griffith, E., and Black, D.M. (2003). TES is a novel focal adhesion protein with a role in cell spreading. J Cell Sci *116*, 897-906.
9. Garvalov, B.K., Higgins, T.E., Sutherland, J.D., Zettl, M., Scaplehorn, N., Köcher, T., Piddini, E., Griffiths, G., and Way, M. (2003). The conformational state of Tes regulates its zyxin-dependent recruitment to focal adhesions. J Cell Biol *161*, 33-39. 10.1083/jcb.200211015.
10. Oldenburg, J., van der Krogt, G., Twiss, F., Bongaarts, A., Habani, Y., Slotman, J.A., Houtsmuller, A., Huveneers, S., and de Rooij, J. (2015). VASP, zyxin and TES are tension-dependent members of Focal Adherens Junctions independent of the α-catenin-vinculin module. Sci Rep *5*, 17225. 10.1038/srep17225.
11. Hadzic, E., Catillon, M., Halavatyi, A., Medves, S., Van Troys, M., Moes, M., Baird, M.A., Davidson, M.W., Schaffner-Reckinger, E., Ampe, C., and Friederich, E. (2015). Delineating the Tes Interaction Site in Zyxin and Studying Cellular Effects of Its Disruption. PLoS One *10*, e0140511. 10.1371/journal.pone.0140511.
12. Zhong, Y., Zhu, J., Wang, Y., Zhou, J., Ren, K., Ding, X., and Zhang, J. (2009). LIM domain protein TES changes its conformational states in different cellular compartments. Mol Cell Biochem *320*, 85-92. 10.1007/s11010-008-9901-7.
13. Sala, S., Catillon, M., Hadzic, E., Schaffner-Reckinger, E., Van Troys, M., and Ampe, C. (2017). The PET and LIM1-2 domains of testin contribute to intramolecular and homodimeric interactions. PLoS One *12*, e0177879. 10.1371/journal.pone.0177879.
14. Griffith, E., Coutts, A.S., and Black, D.M. (2004). Characterisation of chicken TES and its role in cell spreading and motility. Cell Motil Cytoskeleton *57*, 133-142. 10.1002/cm.10162.

15. Ren, D.D., Kelly, M., Kim, S.M., Grimsley-Myers, C.M., Chi, F.L., and Chen, P. (2013). Testin interacts with vangl2 genetically to regulate inner ear sensory cell orientation and the normal development of the female reproductive tract in mice. Dev Dyn *242*, 1454-1465. 10.1002/dvdy.24042.
16. Beckerle, M.C. (1986). Identification of a new protein localized at sites of cell-substrate adhesion. J Cell Biol *103*, 1679-1687.
17. Crawford, A.W., and Beckerle, M.C. (1991). Purification and characterization of zyxin, an 82,000-dalton component of adherens junctions. J Biol Chem *266*, 5847-5853.
18. Hansen, M.D., and Beckerle, M.C. (2006). Opposing roles of zyxin/LPP ACTA repeats and the LIM domain region in cell-cell adhesion. J Biol Chem *281*, 16178-16188. 10.1074/jbc.M512771200.
19. Lee, N.P., Mruk, D.D., Conway, A.M., and Cheng, C.Y. (2004). Zyxin, axin, and Wiskott-Aldrich syndrome protein are adaptors that link the cadherin/catenin protein complex to the cytoskeleton at adherens junctions in the seminiferous epithelium of the rat testis. J Androl *25*, 200-215.
20. Macalma, T., Otte, J., Hensler, M.E., Bockholt, S.M., Louis, H.A., Kalff-Suske, M., Grzeschik, K.H., von der Ahe, D., and Beckerle, M.C. (1996). Molecular characterization of human zyxin. J Biol Chem *271*, 31470-31478.
21. Nguyen, T.N., Uemura, A., Shih, W., and Yamada, S. (2010). Zyxin-mediated actin assembly is required for efficient wound closure. J Biol Chem *285*, 35439-35445. 10.1074/jbc.M110.119487.
22. Vasioukhin, V., Bauer, C., Yin, M., and Fuchs, E. (2000). Directed actin polymerization is the driving force for epithelial cell-cell adhesion. Cell *100*, 209-219.
23. Smith, M.A., Blankman, E., Deakin, N.O., Hoffman, L.M., Jensen, C.C., Turner, C.E., and Beckerle, M.C. (2013). LIM domains target actin regulators paxillin and zyxin to sites of stress fiber strain. PLoS One *8*, e69378. 10.1371/journal.pone.0069378.
24. Smith, M.A., Blankman, E., Gardel, M.L., Luettjohann, L., Waterman, C.M., and Beckerle, M.C. (2010). A zyxin-mediated mechanism for actin stress fiber maintenance and repair. Dev Cell *19*, 365-376. 10.1016/j.devcel.2010.08.008.
25. Yoshigi, M., Hoffman, L.M., Jensen, C.C., Yost, H.J., and Beckerle, M.C. (2005). Mechanical force mobilizes zyxin from focal adhesions to actin filaments and regulates cytoskeletal reinforcement. J Cell Biol *171*, 209-215. 10.1083/jcb.200505018.
26. Hoffman, L.M., Nix, D.A., Benson, B., Boot-Hanford, R., Gustafsson, E., Jamora, C., Menzies, A.S., Goh, K.L., Jensen, C.C., Gertler, F.B., et al. (2003). Targeted disruption of the murine zyxin gene. Mol Cell Biol *23*, 70-79.
27. Rauskolb, C., Pan, G., Reddy, B.V., Oh, H., and Irvine, K.D. (2011). Zyxin links fat signaling to the hippo pathway. PLoS Biol *9*, e1000624. 10.1371/journal.pbio.1000624.
28. Williams-Masson, E.M., Malik, A.N., and Hardin, J. (1997). An actin-mediated two-step mechanism is required for ventral enclosure of the C. elegans hypodermis. Development *124*, 2889-2901.
29. Costa, M., Raich, W., Agbunag, C., Leung, B., Hardin, J., and Priess, J.R. (1998). A putative catenin-cadherin system mediates morphogenesis of the Caenorhabditis elegans embryo. J Cell Biol *141*, 297-308.
30. Priess, J.R., and Hirsh, D.I. (1986). Caenorhabditis elegans morphogenesis: the role of the cytoskeleton in elongation of the embryo. Dev Biol *117*, 156-173.

31. Gally, C., Wissler, F., Zahreddine, H., Quintin, S., Landmann, F., and Labouesse, M. (2009). Myosin II regulation during C. elegans embryonic elongation: LET-502/ROCK, MRCK-1 and PAK-1, three kinases with different roles. Development *136*, 3109-3119. 10.1242/dev.039412.
32. Chisholm, A.D., and Hardin, J. (2005). Epidermal morphogenesis. WormBook, 1-22. 10.1895/wormbook.1.35.1.
33. Vuong-Brender, T.T., Yang, X., and Labouesse, M. (2016). C. elegans Embryonic Morphogenesis. Curr Top Dev Biol *116*, 597-616. 10.1016/bs.ctdb.2015.11.012.
34. Vuong-Brender, T.T., Ben Amar, M., Pontabry, J., and Labouesse, M. (2017). The interplay of stiffness and force anisotropies drives embryo elongation. Elife *6*. 10.7554/eLife.23866.
35. Cox-Paulson, E.A., Walck-Shannon, E., Lynch, A.M., Yamashiro, S., Zaidel-Bar, R., Eno, C.C., Ono, S., and Hardin, J. (2012). Tropomodulin protects alpha-catenin-dependent junctional-actin networks under stress during epithelial morphogenesis. Curr Biol *22*, 1500-1505. 10.1016/j.cub.2012.06.025.
36. Lockwood, C., Zaidel-Bar, R., and Hardin, J. (2008). The C. elegans zonula occludens ortholog cooperates with the cadherin complex to recruit actin during morphogenesis. Curr Biol *18*, 1333-1337. 10.1016/j.cub.2008.07.086.
37. Lynch, A.M., Grana, T., Cox-Paulson, E., Couthier, A., Cameron, M., Chin-Sang, I., Pettitt, J., and Hardin, J. (2012). A Genome-wide Functional Screen Shows MAGI-1 Is an L1CAM-Dependent Stabilizer of Apical Junctions in C. elegans. Curr Biol *22*, 1891-1899. 10.1016/j.cub.2012.08.024.
38. Zaidel-Bar, R., Joyce, M.J., Lynch, A.M., Witte, K., Audhya, A., and Hardin, J. (2010). The F-BAR domain of SRGP-1 facilitates cell-cell adhesion during C. elegans morphogenesis. J Cell Biol *191*, 761-769. 10.1083/jcb.201005082.
39. Kang, H., Bang, I., Weis, W.I., and Choi, H.J. (2016). Purification, crystallization and initial crystallographic analysis of the α-catenin homologue HMP-1 from Caenorhabditis elegans. Acta Crystallogr F Struct Biol Commun *72*, 234-239. 10.1107/s2053230x16001862.
40. Sala, S., Van Troys, M., Medves, S., Catillon, M., Timmerman, E., Staes, A., Schaffner-Reckinger, E., Gevaert, K., and Ampe, C. (2017). Expanding the Interactome of TES by Exploiting TES Modules with Different Subcellular Localizations. J Proteome Res *16*, 2054-2071. 10.1021/acs.jproteome.7b00034.
41. Callaci, S., Morrison, K., Shao, X., Schuh, A.L., Wang, Y., Yates, J.R., Hardin, J., and Audhya, A. (2015). Phosphoregulation of the C. elegans cadherin-catenin complex. Biochem J *472*, 339-352. 10.1042/bj20150410.
42. Cheah, J.S., Jacobs, K.A., Lai, T.W., Caballelo, R., Yee, J.L., Ueda, S., Heinrich, V., and Yamada, S. (2021). Spatial proximity of proteins surrounding zyxin under force-bearing conditions. Mol Biol Cell *32*, 1221-1228. 10.1091/mbc.E19-10-0568.
43. Sala, S., and Oakes, P.W. (2021). Stress fiber strain recognition by the LIM protein testin is cryptic and mediated by RhoA. Mol Biol Cell *32*, 1758-1771. 10.1091/mbc.E21-03-0156.
44. Winkelman, J.D., Anderson, C.A., Suarez, C., Kovar, D.R., and Gardel, M.L. (2020). Evolutionarily diverse LIM domain-containing proteins bind stressed actin filaments through a conserved mechanism. Proc Natl Acad Sci U S A *117*, 25532-25542. 10.1073/pnas.2004656117.

45. Benjamin, J.M., Kwiatkowski, A.V., Yang, C., Korobova, F., Pokutta, S., Svitkina, T., Weis, W.I., and Nelson, W.J. (2010). AlphaE-catenin regulates actin dynamics independently of cadherin-mediated cell-cell adhesion. J Cell Biol *189*, 339-352. 10.1083/jcb.200910041.
46. Drees, F., Pokutta, S., Yamada, S., Nelson, W.J., and Weis, W.I. (2005). Alpha-catenin is a molecular switch that binds E-cadherin-beta-catenin and regulates actin-filament assembly. Cell *123*, 903-915. 10.1016/j.cell.2005.09.021.
47. Griffith, E., Coutts, A.S., and Black, D.M. (2005). RNAi knockdown of the focal adhesion protein TES reveals its role in actin stress fibre organisation. Cell Motil Cytoskeleton *60*, 140-152. 10.1002/cm.20052.
48. Piekny, A.J., Johnson, J.L., Cham, G.D., and Mains, P.E. (2003). The Caenorhabditis elegans nonmuscle myosin genes nmy-1 and nmy-2 function as redundant components of the let-502/Rho-binding kinase and mel-11/myosin phosphatase pathway during embryonic morphogenesis. Development *130*, 5695-5704. 10.1242/dev.00807.
49. Wissmann, A., Ingles, J., and Mains, P.E. (1999). The Caenorhabditis elegans mel-11 myosin phosphatase regulatory subunit affects tissue contraction in the somatic gonad and the embryonic epidermis and genetically interacts with the Rac signaling pathway. Dev Biol *209*, 111-127. 10.1006/dbio.1999.9242.
50. Wissmann, A., Ingles, J., McGhee, J.D., and Mains, P.E. (1997). Caenorhabditis elegans LET-502 is related to Rho-binding kinases and human myotonic dystrophy kinase and interacts genetically with a homolog of the regulatory subunit of smooth muscle myosin phosphatase to affect cell shape. Genes Dev *11*, 409-422.
51. Maiden, S.L., Harrison, N., Keegan, J., Cain, B., Lynch, A.M., Pettitt, J., and Hardin, J. (2013). Specific conserved C-terminal amino acids of Caenorhabditis elegans HMP-1/α-catenin modulate F-actin binding independently of vinculin. J Biol Chem *288*, 5694-5706. 10.1074/jbc.M112.438093.
52. Slabodnick*, M.M., Tintori*, S.C., Prakash, M., Higgins, C.D., Chen, A.H., Cupp, T.D., Wong, T., Bowie, E., Jug, F., and Goldstein, B. (2022). Afadin and zyxin contribute to coupling between cell junctions and contractile actomyosin networks during apical constriction. Submitted.
53. Lecroisey, C., Martin, E., Mariol, M.C., Granger, L., Schwab, Y., Labouesse, M., Ségalat, L., and Gieseler, K. (2008). DYC-1, a protein functionally linked to dystrophin in Caenorhabditis elegans is associated with the dense body, where it interacts with the muscle LIM domain protein ZYX-1. Mol Biol Cell *19*, 785-796. 10.1091/mbc.E07-05-0497.
54. Smith, P., Leung-Chiu, W.M., Montgomery, R., Orsborn, A., Kuznicki, K., Gressman-Coberly, E., Mutapcic, L., and Bennett, K. (2002). The GLH proteins, Caenorhabditis elegans P granule components, associate with CSN-5 and KGB-1, proteins necessary for fertility, and with ZYX-1, a predicted cytoskeletal protein. Dev Biol *251*, 333-347.
55. Diogon, M., Wissler, F., Quintin, S., Nagamatsu, Y., Sookhareea, S., Landmann, F., Hutter, H., Vitale, N., and Labouesse, M. (2007). The RhoGAP RGA-2 and LET-502/ROCK achieve a balance of actomyosin-dependent forces in C. elegans epidermis to control morphogenesis. Development *134*, 2469-2479. 10.1242/dev.005074.
56. Zhang, H., Landmann, F., Zahreddine, H., Rodriguez, D., Koch, M., and Labouesse, M. (2011). A tension-induced mechanotransduction pathway promotes epithelial morphogenesis. Nature *471*, 99-103. 10.1038/nature09765.

57. Chan, B.G., Rocheleau, S.K., Smit, R.B., and Mains, P.E. (2015). The Rho guanine exchange factor RHGF-2 acts through the Rho-binding kinase LET-502 to mediate embryonic elongation in C. elegans. Dev Biol *405*, 250-259. 10.1016/j.ydbio.2015.07.010.
58. Brenner, S. (1974). The genetics of Caenorhabditis elegans. Genetics *77*, 71-94.
59. Dickinson, D.J., Pani, A.M., Heppert, J.K., Higgins, C.D., and Goldstein, B. (2015). Streamlined Genome Engineering with a Self-Excising Drug Selection Cassette. Genetics *200*, 1035-1049. 10.1534/genetics.115.178335.
60. Schwartz, M.L., and Jorgensen, E.M. (2016). SapTrap, a Toolkit for High-Throughput CRISPR/Cas9 Gene Modification in Caenorhabditis elegans. Genetics *202*, 1277-1288. 10.1534/genetics.115.184275.
61. Mello, C., and Fire, A. (1995). Chapter 19 DNA Transformation. Cuenorhubditis elegans: Modern Biologcal Analysis of an Organism. Elsevier BV.
62. Walston, T., Tuskey, C., Edgar, L., Hawkins, N., Ellis, G., Bowerman, B., Wood, W., and Hardin, J. (2004). Multiple Wnt signaling pathways converge to orient the mitotic spindle in early C. elegans embryos. Dev Cell *7*, 831-841. 10.1016/j.devcel.2004.10.008.
63. Albertson, D.G. (1984). Formation of the first cleavage spindle in nematode embryos. Developmental Biology *101*, 61-72. 10.1016/0012-1606(84)90117-9.
64. Leung, B., Hermann, G.J., and Priess, J.R. (1999). Organogenesis of the Caenorhabditis elegans Intestine. Developmental Biology *216*, 114-134. 10.1006/dbio.1999.9471.
65. Edelstein, A., Amodaj, N., Hoover, K., Vale, R., and Stuurman, N. (2010). Computer Control of Microscopes Using μManager. In Current Protocols in Molecular Biology, (Wiley-Blackwell). 10.1002/0471142727.mb1420s92.
66. Edelstein, A.D., Tsuchida, M.A., Amodaj, N., Pinkard, H., Vale, R.D., and Stuurman, N. (2014). Advanced methods of microscope control using μManager software. Journal of Biological Methods *1*, 10. 10.14440/jbm.2014.36.
67. Shao, X., Lucas, B., Strauch, J., and Hardin, J. (2019). The adhesion modulation domain of Caenorhabditis elegans alpha-catenin regulates actin binding during morphogenesis. Mol Biol Cell *30*, 2115-2123. 10.1091/mbc.E19-01-0018.
68. Freeman, G.H., and Halton, J.H. (1951). Note on an exact treatment of contingency, goodness of fit and other problems of significance. Biometrika *38*, 141-149.
69. Bolte, S., and Cordelieres, F.P. (2006). A guided tour into subcellular colocalization analysis in light microscopy. J Microsc *224*, 213-232. 10.1111/j.1365-2818.2006.01706.x.
70. Mayers, J.R., Fyfe, I., Schuh, A.L., Chapman, E.R., Edwardson, J.M., and Audhya, A. (2011). ESCRT-0 assembles as a heterotetrameric complex on membranes and binds multiple ubiquitinylated cargoes simultaneously. J Biol Chem *286*, 9636-9645. 10.1074/jbc.M110.185363.
71. Stiernagle, T. (2006). Maintenance of C. elegans. WormBook, 1-11. 10.1895/wormbook.1.101.1.
72. Zhang, Y., Wang, X., Matakatsu, H., Fehon, R., and Blair, S.S. (2016). The novel SH3 domain protein Dlish/CG10933 mediates fat signaling in Drosophila by binding and regulating Dachs. Elife *5*. 10.7554/eLife.16624.
73. Lecroisey, C., Brouilly, N., Qadota, H., Mariol, M.C., Rochette, N.C., Martin, E., Benian, G.M., Ségalat, L., Mounier, N., and Gieseler, K. (2013). ZYX-1, the unique zyxin protein

of Caenorhabditis elegans, is involved in dystrophin-dependent muscle degeneration. Mol Biol Cell *24*, 1232-1249. 10.1091/mbc.E12-09-0679.

Figure 1

Figure 1

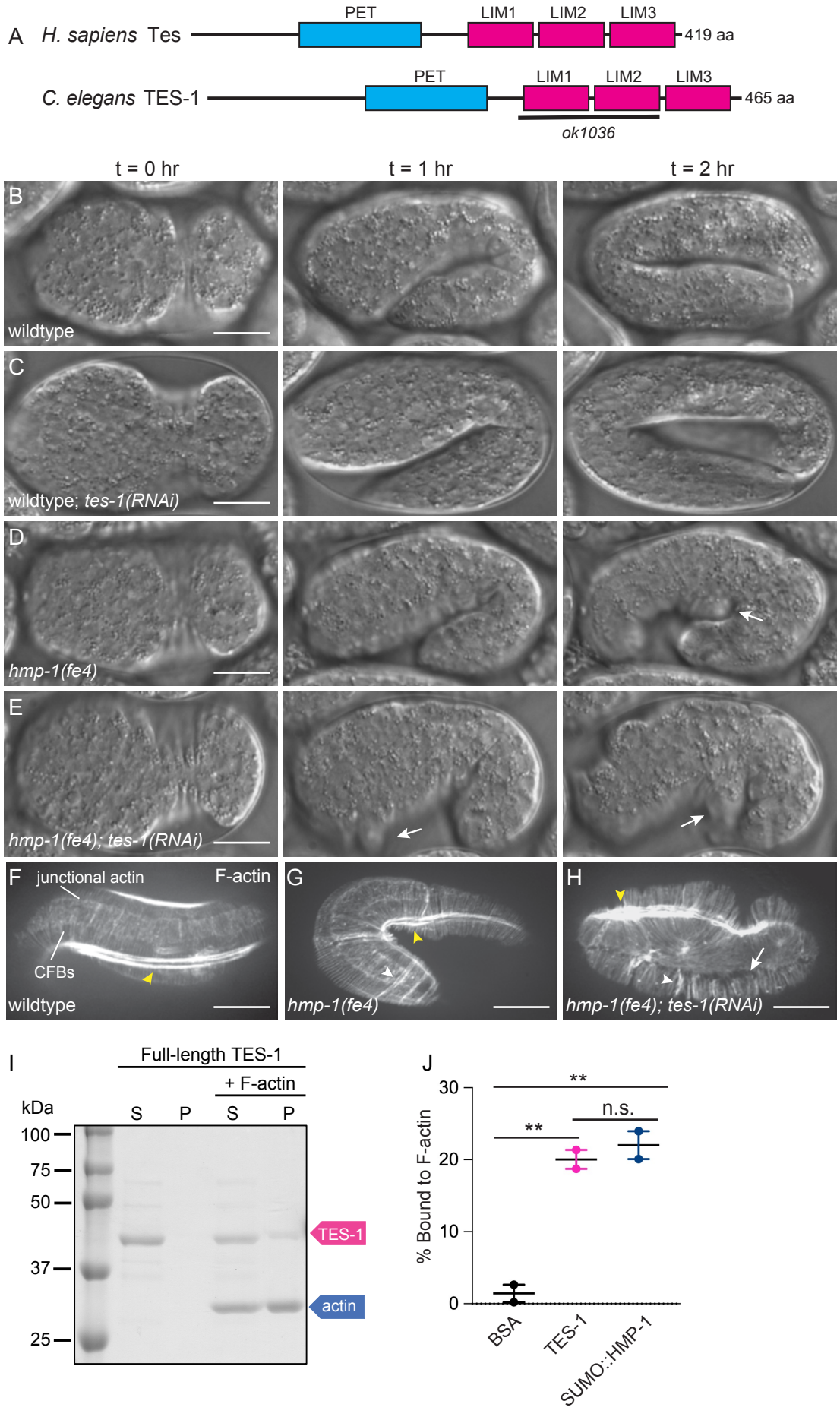

Figure 2

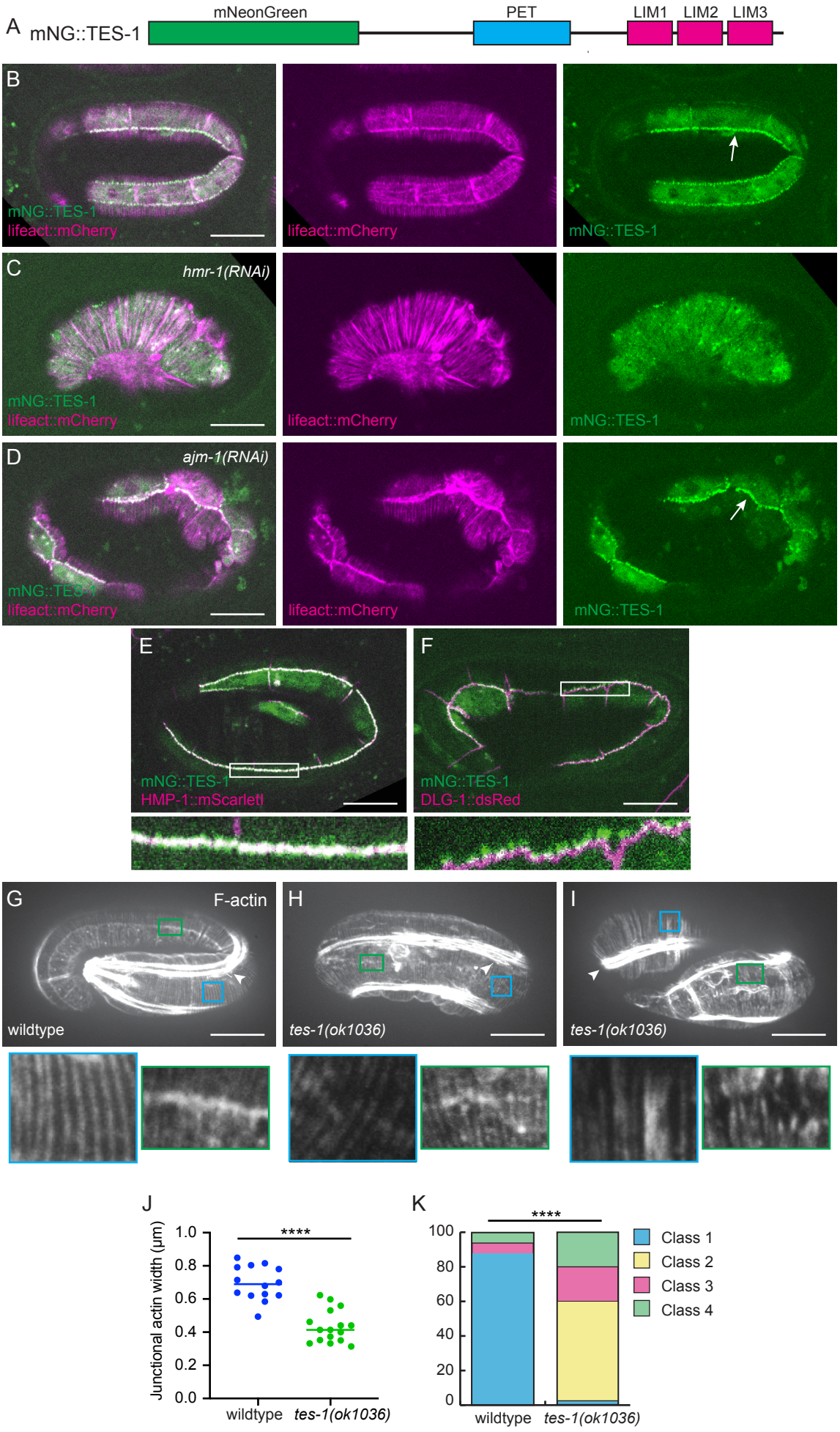
A
mNG::TES-1
mNeonGreen
PET
LIM1
LIM2
LIM3
B
mNG::TES-1
lifeact::mCherry
lifeact::mCherry
mNG::TES-1
C
hmr-1(RNAi)
mNG::TES-1
lifeact::mCherry
lifeact::mCherry
mNG::TES-1
D
ajm-1(RNAi)
mNG::TES-1
lifeact::mCherry
lifeact::mCherry
mNG::TES-1
E
mNG::TES-1
HMP-1::mScarletI
F
mNG::TES-1
DLG-1::dsRed
G
F-actin
wildtype
H
tes-1(ok1036)
I
tes-1(ok1036)
J
Junctional actin width (µm)
1.0
0.8
0.6
0.4
0.2
0.0
****
wildtype
tes-1(ok1036)
K
100
80
60
40
20
0
****
Class 1
Class 2
Class 3
Class 4
wildtype
tes-1(ok1036)

Figure 3

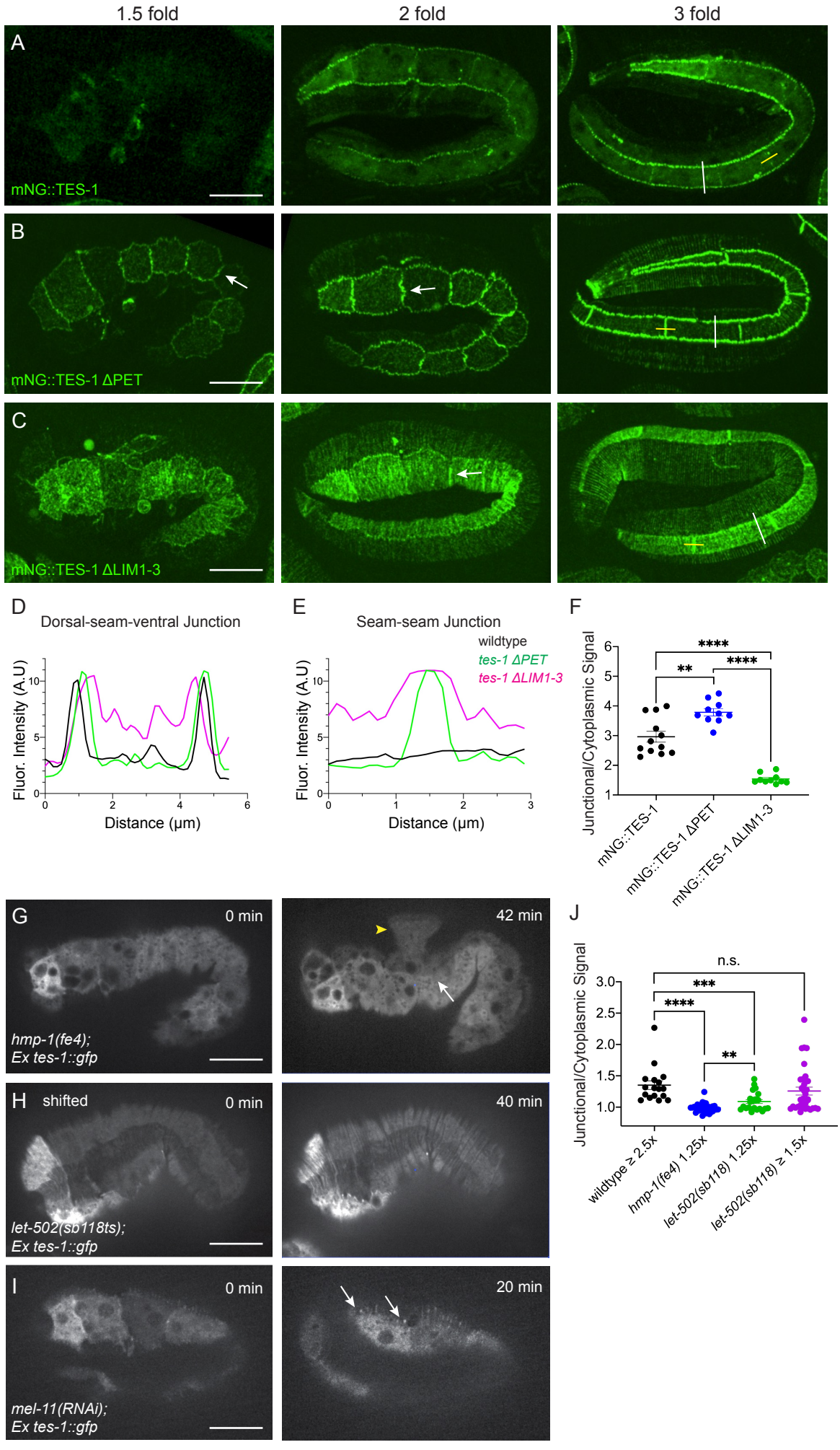
1.5 fold
2 fold
3 fold
A
mNG::TES-1
B
mNG::TES-1 ΔPET
C
mNG::TES-1 ΔLIM1-3
D
Dorsal-seam-ventral Junction
Fluor. Intensity (A.U)
Distance (μm)
E
Seam-seam Junction
wildtype
tes-1 ΔPET
tes-1 ΔLIM1-3
Fluor. Intensity (A.U)
Distance (μm)
F
Junctional/Cytoplasmic Signal
****
**
****
mNG::TES-1
mNG::TES-1 ΔPET
mNG::TES-1 ΔLIM1-3
G
0 min
42 min
hmp-1(fe4);
Ex tes-1::gfp
H
shifted
0 min
40 min
let-502(sb118ts);
Ex tes-1::gfp
I
0 min
20 min
mel-11(RNAi);
Ex tes-1::gfp
J
Junctional/Cytoplasmic Signal
n.s.
***
****
**
wildtype ≥ 2.5x
hmp-1(fe4) 1.25x
let-502(sb118) 1.25x
let-502(sb118) ≥ 1.5x

Figure 4

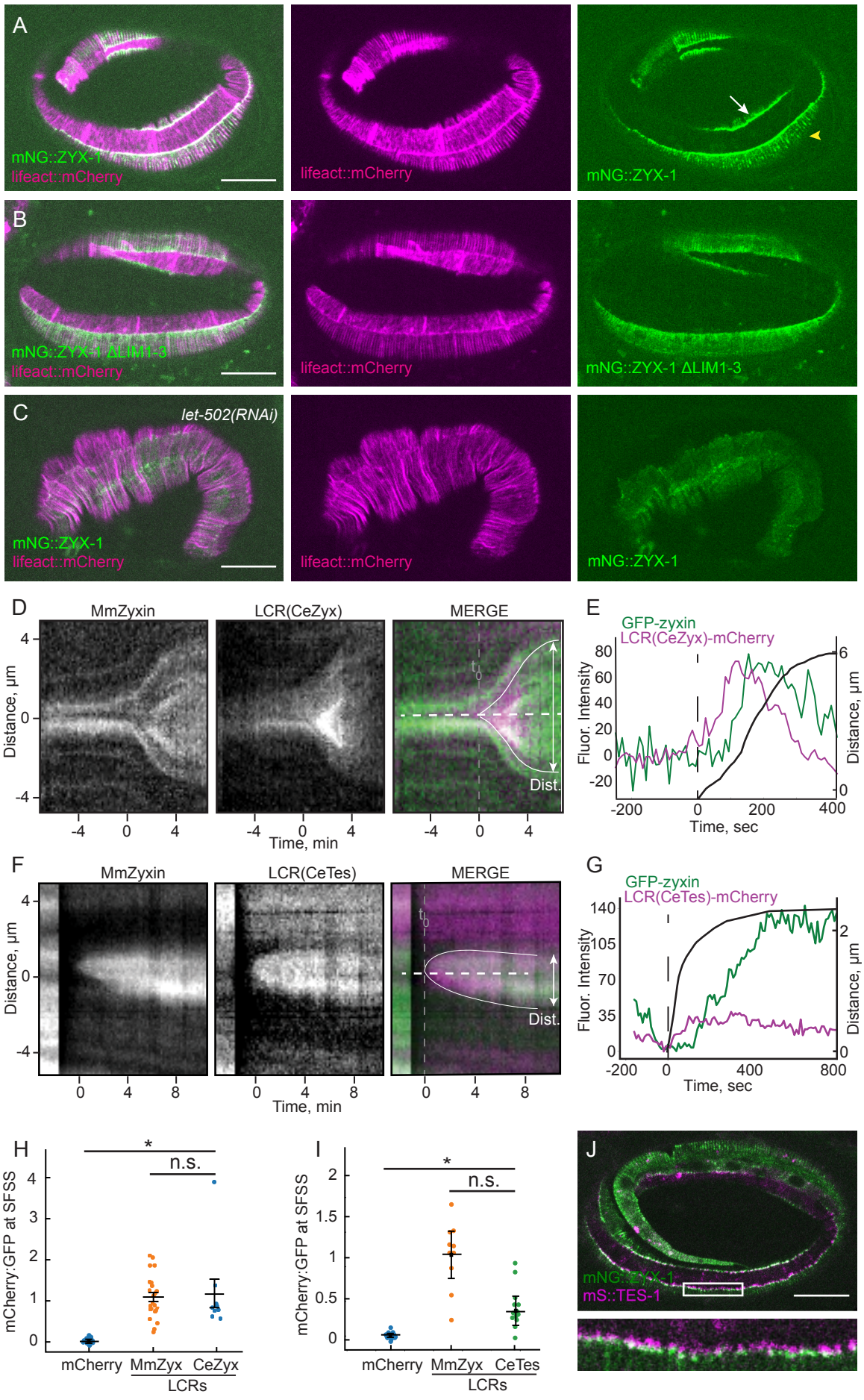
A
mNG::ZYX-1
lifeact::mCherry
lifeact::mCherry
mNG::ZYX-1
B
mNG::ZYX-1 ΔLIM1-3
lifeact::mCherry
lifeact::mCherry
mNG::ZYX-1 ΔLIM1-3
C
let-502(RNAi)
mNG::ZYX-1
lifeact::mCherry
lifeact::mCherry
mNG::ZYX-1
D
MmZyxin
LCR(CeZyx)
MERGE
Distance, µm
Time, min
Dist.
E
GFP-zyxin
LCR(CeZyx)-mCherry
Fluor. Intensity
Distance, µm
Time, sec
F
MmZyxin
LCR(CeTes)
MERGE
Distance, µm
Time, min
Dist.
G
GFP-zyxin
LCR(CeTes)-mCherry
Fluor. Intensity
Distance, µm
Time, sec
H
mCherry:GFP at SFSS
*
n.s.
mCherry
MmZyx
CeZyx
LCRs
I
mCherry:GFP at SFSS
*
n.s.
mCherry
MmZyx
CeTes
LCRs
J
mNG::ZYX-1
mS::TES-1

Strains used in this study

Strain	Genotype
N2	wildtype
HR1157	*let-502(sb118ts)I*
LP810	*zyx-1(cp415[mNG-C1::zyx-1a])II*
LP831	*zyx-1Δ(cp419[Pmyo-2>GFP])II*
ML1651	*mcIs46 [dlg-1::RFP + unc-119(+)]*
MQ468	*hmp-2(qm39)I*
PE532	*xnIs96[pJN455(hmr-1p::hmr-1::GFP::unc-54 3'UTR) + unc-119(+)]*
PE633	*feEx324[zyx-1::mCherry rol-6(su1006)]*
PE636	*feEx327[zyx-1::gfp Pmyo-2::dTomato]*
PE644	*zyx-1(gk190)II, feEx327[zyx-1::gfp myo-2p::dTomato]*
PE647	*zyx-1(gk190)II, hmp-1(fe4)/nT1V, feEx328[zyx-1D376-603::gfp myo-2p::dTomato]*
PE649	*zyx-1(gk190)II, hmp-1(fe4)/nT1V, feEx329[zyx-1D479-603::gfp myo-2p::dTomato]*
PE650	*zyx-1(gk190)II, hmp-1(fe4)/nT1V, feEx330[zyx-1D526-603::gfp myo-2p::dTomato]*
PE651	*zyx-1(gk190)II, hmp-1(fe4)/nT1V, feEx331[zyx-1D166-200::gfp myo-2p::dTomato]*
PE671	*mcIs46[dlg-1::RFP + unc-119(+)], feEx327[zyx-1::gfp myo-2p::dTomato]*
PE97	*hmp-1(fe4)V*
PHX5560	*zyx-1(syb5560[mNG::zyx-1a, deltaLIM1-3])II*
PHX5622	*tes-1(syb5622[mNG::FLAG::tes-1, deltaLIM1-3])IV*
PHX5627	*tes-1(syb5622[mNG::FLAG::tes-1, deltaPET])IV*
SU1042	*tes-1(jc71[mNeonGreen::tes-1])IV; zyx-1(gk190)II*
SU1043	*tes-1(jc71[mNeonGreen::tes-1])IV; mcEX40[plin-26::vab-10::mcherry; myo-2::gfp])IV*
SU1044	*tes-1(jc71[mNeonGreen::tes-1])IV; curIs[plin-26::lifeact::mcherry::unc-54 3'UTR; unc-119(+)]*
SU1058	*tes-1(jc71[mNG::tes-1])IV; zyx-1(null, replaced with Pmyo-2::gfp)II*
SU1072	*tes-1(jc71[mNG::FLAG::tes-1])IV; hmp-1(jc58[hmp-1::mScarlet-I+LoxP511])V*
SU1073	*zyx-1(null, replaced with Pmyo-2::gfp)II; tes-1(ok1036)IV*
SU1085	*tes-1(jc110[mScarlet-I::FLAG::tes-1+LoxP511])IV*
SU1087	*zyx-1(mNG::zyx-1a)II; curIs[plin-26::lifeact::mcherry::unc-54 3'UTR; unc-119(+)]*
SU1088	*zyx-1(syb5560[mNG::zyx-1a, deltaLIM1-3])II; curIs[plin-26::lifeact::mcherry::unc-54 3'UTR; unc-119(+)]*
SU1090	*tes-1(jc110[mScarlet-I::FLAG::tes-1+LoxP511])IV; zyx-1(syb5560[mNG::zyx-1a, deltaLIM1-3])II*
SU1091	*tes-1(jc110[mScarlet-I::FLAG::tes-1+LoxP511])IV; zyx-1(mNG::zyx-1a)II*

SU1094	*zyx-1(mNG::zyx-1a)II; tes-1(ok1036)IV*
SU1100	*zyx-1(gk190)II; curIs[plin-26::lifeact::mcherry::unc-54 3'UTR; unc-119(+)]*
SU1101	*tes-1(syb5622[mNG::FLAG::tes-1, deltaLIM1-3])IV; curIs[plin-26::lifeact::mcherry::unc-54 3'UTR; unc-119(+)]*
SU1107	*zyx-1(null, replaced with Pmyo-2::gfp)II; tes-1(syb5622[mNG::FLAG::tes-1, deltaLIM1-3])IV*
SU496	*WT; jcEx159 [5kbptes-1::tes-1::gfp; pRF4; F35D3]*
SU708	*N2; jcEx229[pRF4; Ptes-1::tes-1deltaPET::gfp F2-8; F35D3]*
SU710	*N2; jcEx231[pRF4; Ptes-1::tes-1deltaLIM1::gfp; F35D3]*
SU713	*N2; jcEx234[pRF4; Ptes-1::tes-1deltaLIM2::gfp F2-7; F35D3]*
SU714	*N2; jcEx235[pRF4; Ptes-1::tes-1deltaLIM3::gfp; F35D3]*
SU715	*N2; jcEx236[pRF4; Ptes-1::tes-1deltaLIM1-3::gfp; F35D3]*
SU896	*hmp-1(jc58[hmp-1::mScarlet-I + Lox511])V*
SU931	*curIs[plin-26::lifeact::mcherry::unc-54 3'UTR; unc-119(+)]*
SU955	*tes-1(jc71[mNG::FLAG::tes-1])IV*
VC299	*zyx-1(gk190)II*
VC696	*tes-1(ok1036)IV*

Supplemental Table 2
Primer sequences for CRISPR experiments performed in this study

tes-1 N-terminal 5' Homology arm Forward Primer	5'-GGCTGCTCTTCgTGGtttcttacctattttaaaatgacacctgcc-3'
tes-1 N-terminal 5' Homology arm Reverse Primer	5'-GGGTGCTCTTCgCATCATtactgaaattaattggcatttaacgct-3'
tes-1 N-terminal 3' Homology arm Forward Primer	5'- GGCTGCTCTTCgACGACCGACGTCACGTCTCCCGTTGTtGAC-3'
tes-1 N-terminal 3' Homology arm Reverse Primer	5'- GGGTGCTCTTCgTACGTCTGGAAGTGGTGCCCACGCATAC-3'
tes-1 N-terminal sgRNA	5'- GCACGGCTTCTCGTCCACAA-3'

Figure S1

Supplemental Figure 1

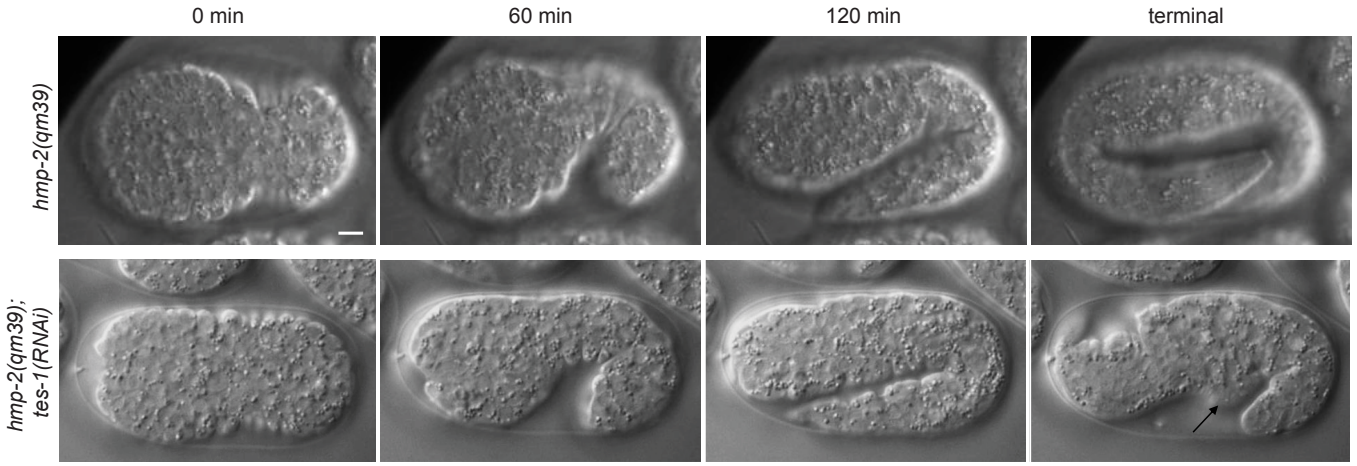

Figure S2

Supplemental Figure 2

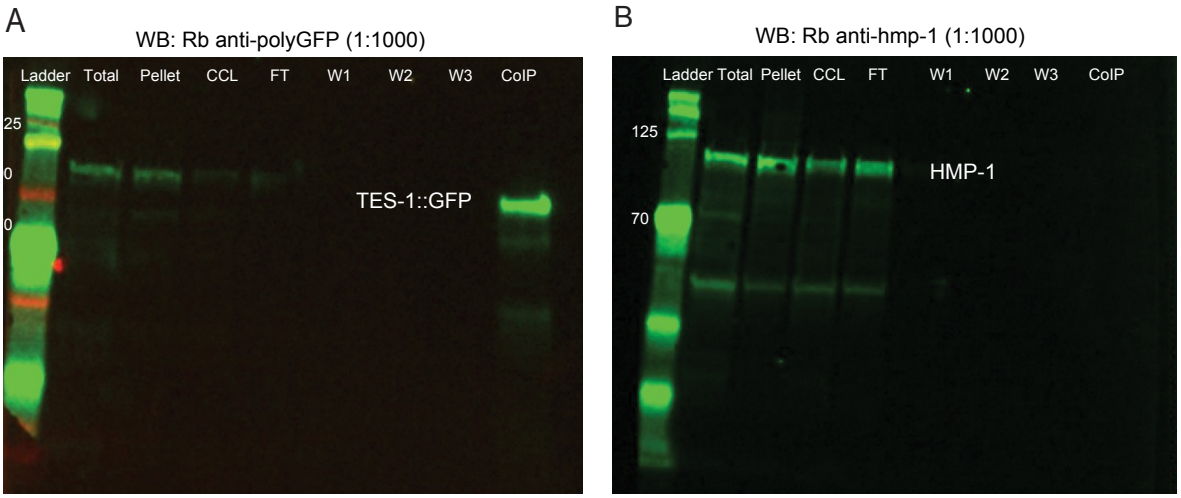

Figure S3

Supplemental Figure 3

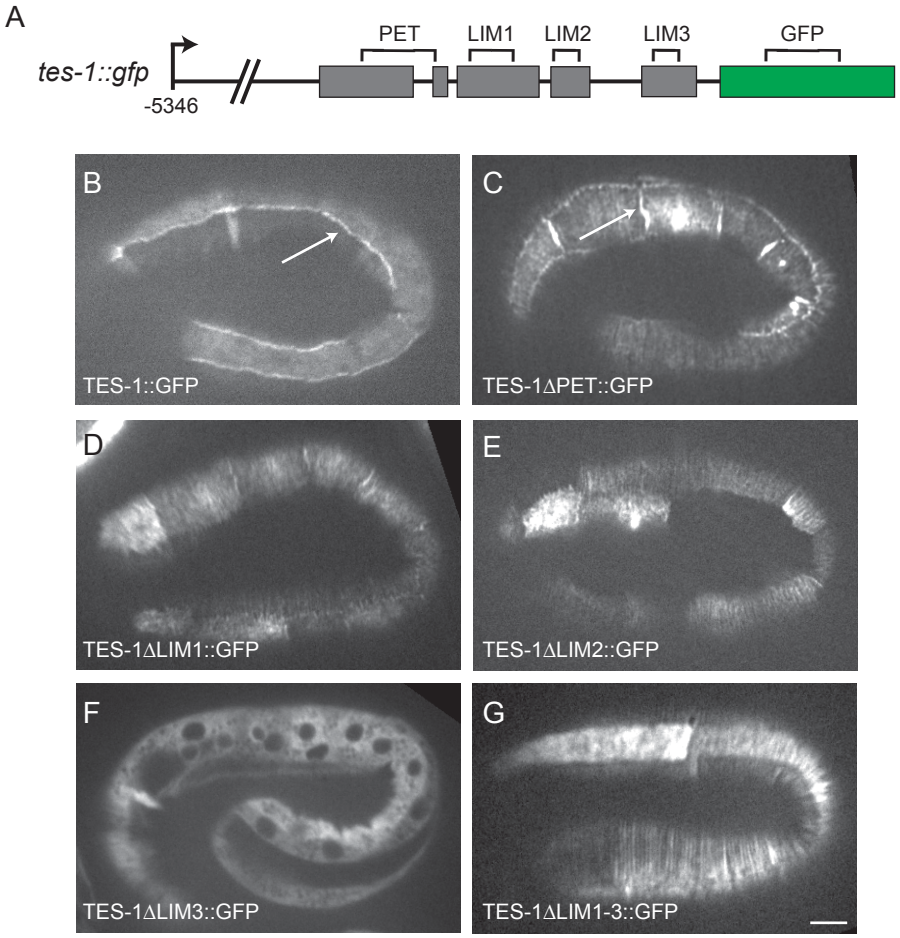

H

Transgene*	Lethal	Survival	% lethal
ok1036; fe4/+	30	46	39.5
+ ΔPET	24	98	19.7**
+ ΔLIM1-3	23	46	33.3
+ ΔLIM2	27	54	33.3
+ ΔLIM3	58	110	34.5

*Stable lines could not be recovered for ΔLIM1, see results
**Significantly different, $p<0.05$, Fisher's Exact Test

Figure S4

Supplemental Figure 4

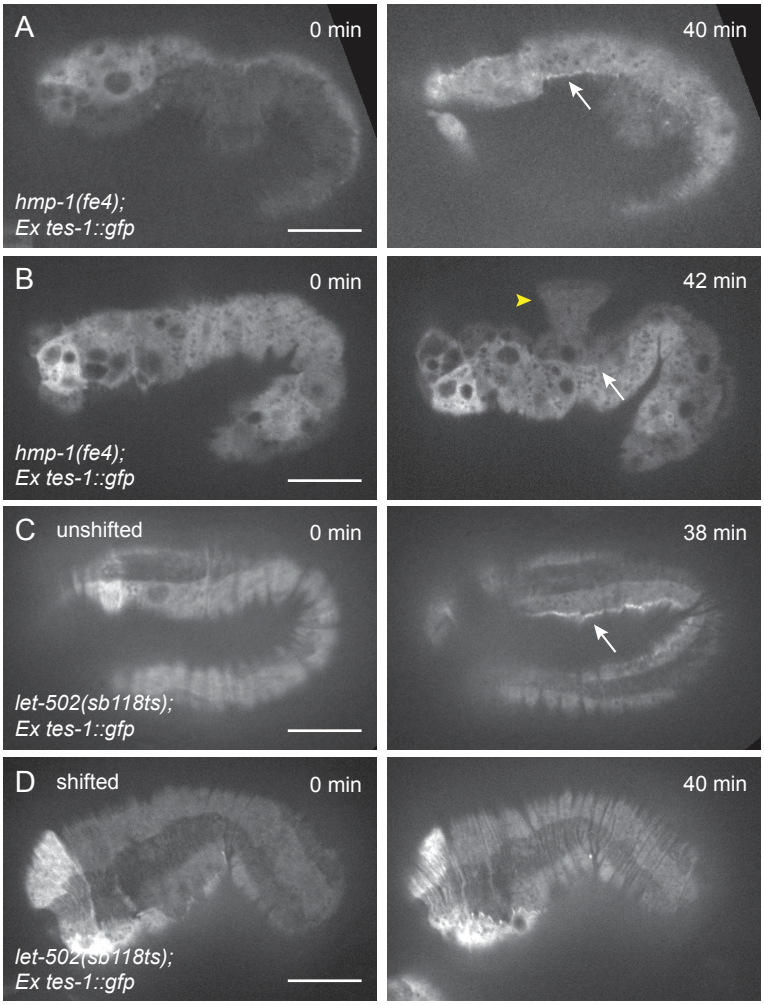

Figure S5

Supplemental Figure 5

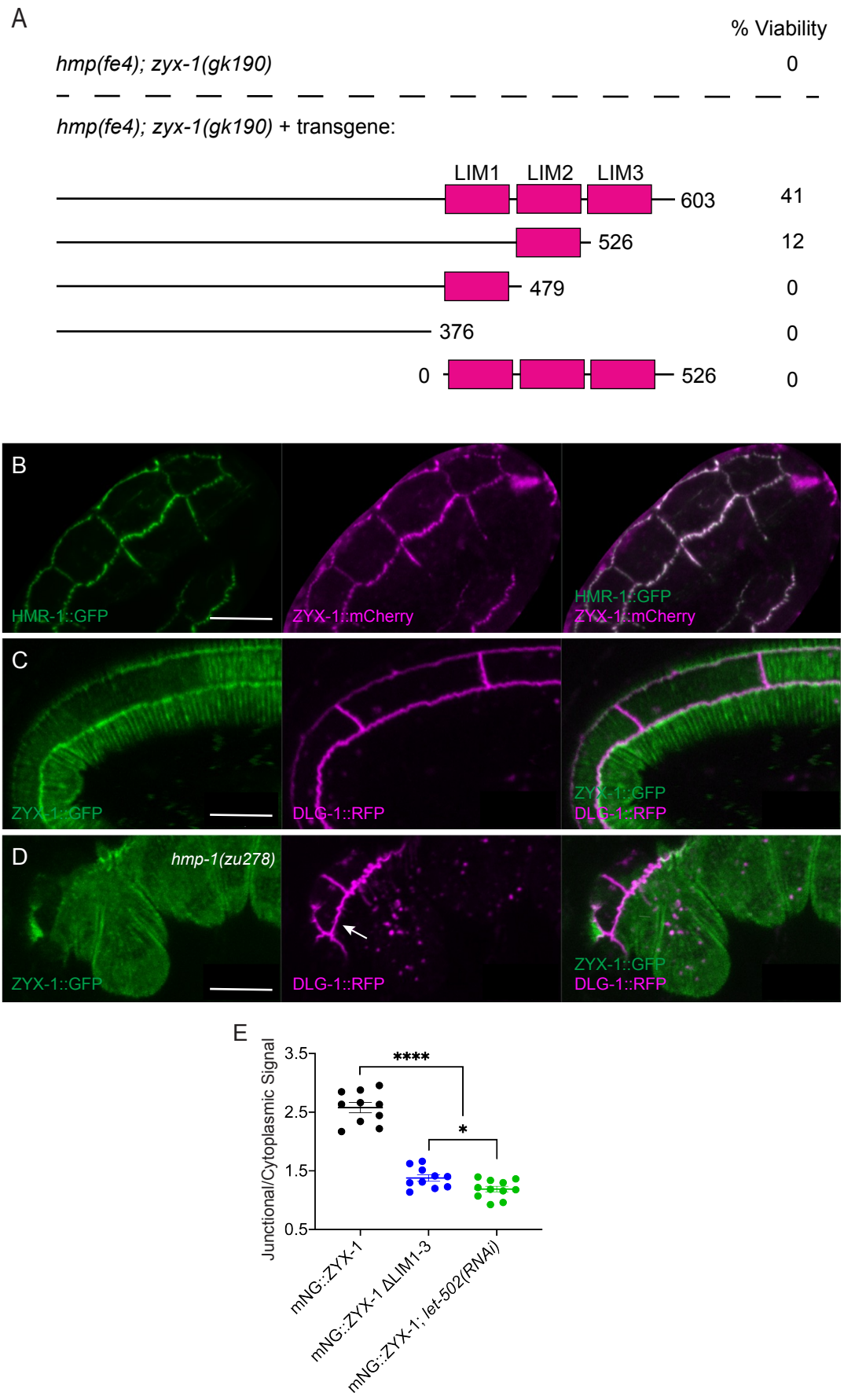

Figure S6

Supplemental Figure 6

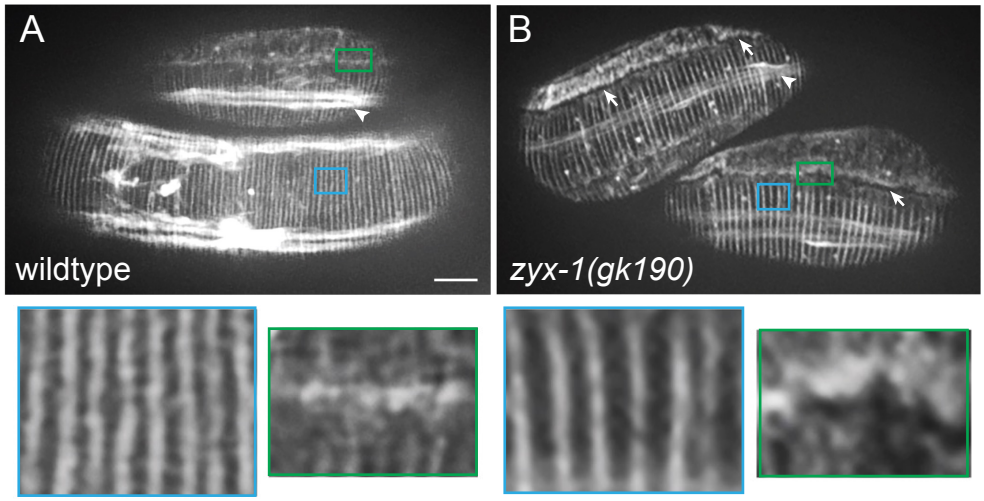

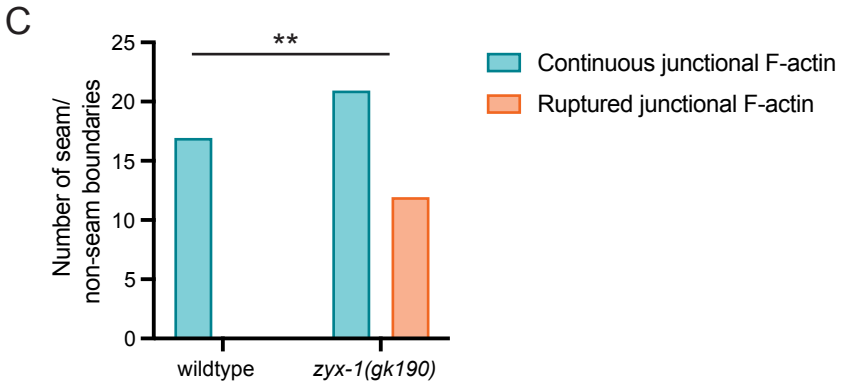

Figure S7

Supplementary Figure 7

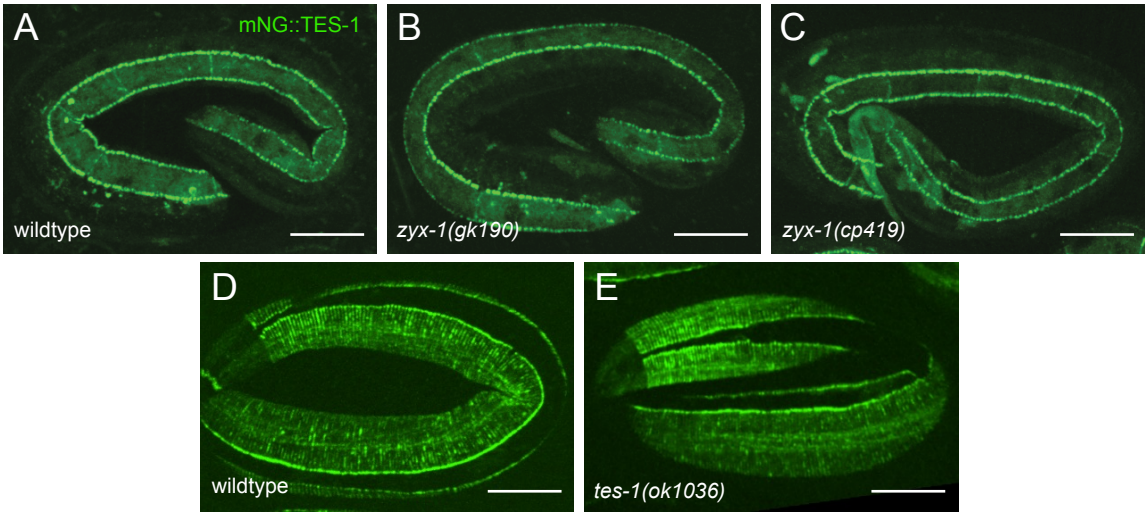

Figure S8

Supplemental Figure 8